https://doi.org/10.5194/bg-2023-15
Preprint. Discussion started: 1 March 2023

Biogeosciences Discussions

Historical dynamics of terrestrial carbon during 1901-2016 as simulated by the CLM-Microbe model

Liyuan He[1], Jorge L. Mazza Rodrigues[2], Melanie A. Mayes[3], Chun-Ta Lai[1], David A. Lipson[1], Xiaofeng Xu*[1]

1. Biology Department, San Diego State University, San Diego, CA, 92182, USA
2. Department of Land, Air and Water Resources, University of California - Davis, Davis, CA 95616, USA
3. Environmental Sciences Division and Climate Change Science Institute, Oak Ridge National Laboratory, Oak Ridge, Tennessee, 37831, USA

Correspondence: Xiaofeng Xu (xxu@sdsu.edu)

Abstract. The CLM-Microbe model was able to reproduce the variations of gross (GPP) and net (NPP) primary productivity, heterotrophic (HR), and soil (SR) respiration, microbial (MBC) biomass C in fungi (FBC) and bacteria (BBC) in the top 30 cm and 1 m, dissolved (DOC) and soil organic C (SOC) in the top 30 cm and 1 m during 2901-2016. During the study period, simulated C variables increased by approximately 30 PgC yr^{-1} for GPP, 13 PgC yr^{-1} for NPP, 12 PgC yr^{-1} for HR, 25 PgC yr^{-1} for SR, 1.0 PgC for FBC and 0.4 PgC for BBC in 0-30 cm, 1.2 PgC for FBC, 0.7 PgC for BBC, 2.4 PgC for DOC, 34 PgC for SOC, and 4 PgC for litter C in 0-1 m, and 37 PgC for vegetation C. Increases in C fluxes and pools were larger at northern high latitudes and in equatorial regions than at other latitudes; the largest absolute increases of C fluxes and pools were in Asia and South America, particularly in eastern Asia and central and northern South America. However, the largest relative increases of GPP, NPP, HR, and SR in Asia and Europe, FBC (0-30 cm and 0-1 m) in South America, BBC (0-30 cm and 0-1 m) in Europe, DOC (0-1 m) in South America and Europe, SOC (0-1 m) in Africa, and vegetation C and litter C (0-1 m) in Europe. Vegetation productivity was primarily controlled by warming and precipitation, while microbial and soil C was jointly governed by vegetation C input and soil temperature and moisture. This study enhances our understanding of soil microbial roles in the global terrestrial C cycle.

1 Introduction

The atmospheric concentration of carbon dioxide (CO_2) has been drastically increased due to fossil fuel combustion and land-use change since the Industrial Revolution (IPCC, 2001, 2013; Lal, 2004, 2008). The radiative forcing caused by the CO_2 enrichment in the atmosphere has led to an increase in the global surface temperature, known as climate warming (IPCC, 2001). Meanwhile, growing gaseous forms of nitrogen (N) in the atmosphere due to anthropogenic activities, including agriculture and fossil fuel combustion, have accelerated atmospheric N inputs into terrestrial ecosystems (Galloway et al., 2008; Van Damme et al., 2021). The increases of atmospheric CO_2, surface temperature, atmospheric particles, and N deposition have induced cascading environmental issues and disrupted carbon (C) and nutrient cycles (Matson et al., 2002; Meeran et al., 2021; Soong et al., 2021).

https://doi.org/10.5194/bg-2023-15
Preprint. Discussion started: 1 March 2023

Previous studies have assessed the effects of increasing atmospheric CO_2, global mean temperature, and N deposition on the global C cycle using Earth system models (ESMs) (Bonan et al., 2019; Todd-Brown et al., 2013). For example, Bonan et al. (2019) compared vegetation productivity, heterotrophic respiration, and vegetation and soil C stocks in the Community Land Model (CLM) forced by two climate reconstructions (CRUNCEPv7 and GSWP3v1) (Dirmeyer et al., 2006; Viovy, 2018). These models, however, were developed with an implicit representation of microbial processes. Given the critical role that soil microorganisms play in soil biogeochemical processes and their sensitivity to environmental changes, explicit incorporation of soil microbial processes into ESMs is essential to improve the prediction of global C cycling (He et al., 2021; Wang et al., 2015; Wang et al., 2017; Wieder et al., 2013). Recently, researchers have applied microbial-explicit models in investigating responses of global C cycle to environmental change. For example, Wieder et al. (2015) have examined the responses of soil, vegetation, and litter C pools to environmental change using the MIMICS model. Wang et al. (2017) also investigated the impacts of environmental change on enzymes, soil, and microbial biomass C pools using the TRIPLEX-MICROBE model. However, the implicit validation of microbial biomass at global or biome levels may introduce uncertainties in the model, particularly in soil microbial biomass and microbe-mediated processes, which can further affect the predicted soil C cycle in those models.

Fungi and bacteria, the two major soil microbial groups, respond differently to environmental change, and differences in their physiological traits concerning biogeochemical processes have been incorporated into the CLM-Microbe model (He et al., 2021; He et al., 2021). Therefore, validating fungal and bacterial biomass in the CLM-Microbe model at fine scales can reduce uncertainties in model predictions. Fungi and bacteria are highly responsive to environmental change; however, their responses differ. For example, fungi decrease more than bacteria under N fertilization (Demoling et al., 2008), whereas fungi are less sensitive than bacteria to water stress (Manzoni et al., 2012). Changes in fungal and bacterial populations can primarily affect terrestrial C cycling considering their distinct roles in biogeochemical processes such as the decomposition of organic materials (Bailey et al., 2002; Boer et al., 2005; Hršelová et al., 1999). Predicting changes in the spatial pattern of fungi and bacteria at the global scale and identifying their controls is essential for understanding the impacts of environmental changes on the global terrestrial C cycle.

To fill the gaps, we investigated the effects of environmental change (climate change, N deposition, rising CO_2, and aerosols) on the global C cycle using the CLM-Microbe model. The CLM-Microbe model, mechanistically representing soil microbial community dynamics by differentiating fungal and bacterial physiology, provides a feasible way to investigate the effects of environmental change on soil C cycling mediated by soil microbes (He et al., 2021). In this study, we aimed to investigate the effects of environmental change on the global C cycle from 1901 to 2016. We first evaluated the performance of the CLM-Microbe model in reproducing soil, vegetation, and microbial C variables, including gross (GPP) and net (NPP) primary productivity, fungal

https://doi.org/10.5194/bg-2023-15
Preprint. Discussion started: 1 March 2023

(FBC) and bacterial (BBC) biomass C in the top 30 cm and 1 m, heterotrophic (HR) and soil (SR) respiration, and dissolved (DOC) and soil (SOC) organic C in the top 30 cm and 1 m. Then, we investigated the effects of environmental change on the temporal trend of variables related to soil, vegetation, microbial, and litter C, including GPP, NPP, HR, SR, FBC, and BBC in the top 30 cm, FBC, BBC, DOC, SOC, and litter C (LitC) in the top 1 m, and vegetation C (VegC) from 1901 to 2016. Finally, we investigated spatial patterns and external environmental controls of changes in those fluxes and pools from 1901 to 2016.

2 Materials and methods

2.1 Model representation of fungal and bacterial biomass

The CLM-Microbe model was built on the model framework developed by Xu et al. (2014) and the default CLM4.5 (hereafter CLM4.5) (Koven et al., 2013). It has been coupled with a microbial functional group–based methane module (Wang et al., 2022; Wang et al., 2019; Xu et al., 2015) and applied to quantify the fungal and bacterial biomass dynamics in natural ecosystems (He et al., 2021). Taken together, the CLM-Microbe model has unique module of microbe-mediated decomposition cascades and microbial functional group-mediated methane cycle, with rest biochemical processes and all biophysical and landscape processes the same with the CLM4.5. The CLM4.5 classifies litter into three pools, i.e., litter 1 (labile), litter 2 (cellulose), and litter 3 (lignin), and soil organic matter (SOM), materials left during later stages of organic C decay, into four pools, i.e., SOM 1, SOM 2, SOM 3, and SOM 4 (low-high recalcitrance). The three litter pools and four SOM pools differ in base decomposition rate (τ), with turnover times of litter pools ranging from 20 hours to 71 days and turnover times of SOM pools ranging from 14 days to 27 years (Fig. S1). Coarse woody debris (CWD) is fragmented, decomposed, and gradually transferred into litter pools and further from litter to SOM pools (Thornton et al. 2007; Koven et al. 2013). In addition to eight C pools (three litter, four SOM, and CWD pools) in the CLM4.5, we introduced dissolved organic matter (DOM) and fungal and bacterial biomass pools in the CLM-Microbe model. The code for the CLM-Microbe model has been archived at https://github.com/email-clm/clm-microbe since 2015. The model version used in this study was checked out on May 1, 2021, with a git commit ID/hash of 222d3bb865a42d71a94d9dc30bd390a6b085ab50, and was archived at Xu et al. (2022).

In the CLM-Microbe model, fungal and bacterial biomasses are the balance of C input from the decomposition of SOM, DOM, and litter and C loss through microbial lysis and microbial respiration. Specifically, fungi and bacteria receive C through the transitions from litter, DOM, and SOM pools; fungi and bacteria lose C through the transitions from fungal and bacterial biomass pools to DOM and SOM pools and the atmosphere. The conceptual diagram of the CLM-Microbe model and major parameters are in Fig. S1 and Table S1, respectively.

https://doi.org/10.5194/bg-2023-15
Preprint. Discussion started: 1 March 2023

The decomposition rates of SOM, DOM, and litter are controlled by both their potential decomposition rates and environmental conditions. The decomposition processes in the CLM-Microbe model are defined following the below equations,

$$D_C = k \times r_{depth} \times r_{tsoil} \times r_{water} \times r_{O_2} \quad \text{equation (1)}$$

$$r_{depth} = \exp\left(-\frac{z}{z_\tau}\right) \quad \text{equation (2)}$$

$$r_{tsoil} = Q_{10}^{\frac{T_{soil,j}-T_{ref}}{10}} \quad \text{equation (3)}$$

$$r_{water} = \begin{cases} 0 & for\ \varphi_j < \varphi_{min} \\ \frac{log\left(\varphi_{min}/\varphi_j\right)}{log\left(\varphi_{min}/\varphi_{max}\right)} & for\ \varphi_{min} \le \varphi_j \le \varphi_{max} \\ 1 & for\ \varphi_j > \varphi_{max} \end{cases} \quad \text{equation (4)}$$

$$r_{O_2} = f_r \times (1 - f_{inun}) \times max\left(O_{2_{unsat}}, O_{2_{min}}\right) + f_{inun} \times max\left(O_{2_{sat}}, O_{2_{min}}\right) \quad \text{equation (5)}$$

where D_C is the rate of substrate (e.g., SOM, DOM, and litter) breakdown (in per day); k is the potential decomposition rate (in per day); r_{O_2} represents the environmental modifier determined by soil oxygen concentration (unitless); r_{depth} is the environmental modifier determined by soil depth (unitless); r_{water} is environmental modifier determined by soil moisture (unitless); r_{tsoil} means the environmental modifier determined by soil temperature (unitless); z means soil depth (in m); z_τ is the e-folding depth for decomposition (in m); $T_{soil,j}$ is soil temperature at layer j (in Kelvin); T_{ref} is the reference temperature for decomposition (in Kelvin), which is set as a Kelvin temperature equals to 25°C; Q_{10} indicates the temperature dependence of decomposition, it is the ratio of the rate at a specific temperature to that at 10°C lower (unitless); Ψ_j is the soil water potential in layer j (in MPa); Ψ_{min} is a lower limit for soil water potential control on decomposition rate (set to -10 MPa), r_{water} will be set as 0 if Ψ_j is lower than Ψ_{min} (in MPa); Ψ_{max} is the upper limit for soil water potential control on decomposition, which equals to the saturated soil matric potential, r_{water} will be set as 1 if Ψ_j is higher than Ψ_{max}; $w_{soil,j}$ means soil water content in layer j (in MPa); f_r is the rooting fraction by soil depth (unitless); f_{inun} means the fraction of inundated area (unitless); $O_{2_{unsat}}$ represents the oxygen available to that demanded by roots and aerobic microbes in unsaturated area (unitless); $O_{2_{min}}$ denotes the ratio between minimum anaerobic decomposition rate and potential aerobic decomposition rate in soil (set to 0.2) (unitless); $O_{2_{sat}}$ represents the oxygen available to that demanded by roots and aerobic microbes in saturated area (unitless); r_{O_2} will be set as 1 in oxic conditions, while it will be estimated as the weighted average of oxygen stress in saturated and unsaturated areas in anoxic conditions (unitless).

Fungi and bacteria have different turnover times, hence, different lysis rate constants were adopted for fungi and bacteria in the CLM-Microbe model (He et al., 2021). In addition, bacterial and fungal growth is highly sensitive to environmental conditions, such as soil moisture and temperature. As a result, in the CLM-Microbe model, fungal and bacterial biomass lysis is mechanistically represented as the interactive effects of their lysis rate constants and environmental factors, i.e., r_{O_2}, r_{water}, r_{tsoil}, and r_{depth}, as

https://doi.org/10.5194/bg-2023-15
Preprint. Discussion started: 1 March 2023

described above. Microbial respiration is widely affected by multiple abiotic and biotic factors, such as substrate concentration and availability, soil moisture, and soil temperature (Gomez-Casanovas et al., 2012; Zhang et al., 2013). Therefore, in the CLM-Microbe model, fungal and bacterial respirations are represented as the interactive effects of substrate (i.e., DOM, SOM, and litter), environmental factors (i.e., r_{O_2}, r_{water}, and r_{tsoil}), and fraction factors quantifying C being respired by fungi and bacteria in transitions (Table S1). Fungal and bacterial biomass turnover and microbial respiration are defined following equations as below,

$$L = k_M \times r_{depth} \times r_{tsoil} \times r_{water} \times r_{O_2} \quad \text{equation (6)}$$

$$R = D_C \times f_{resp} \quad \text{equation (7)}$$

where L denotes the lysis rate of fungal and bacterial biomass (in per day); k_M is the potential turnover rate of fungal (k_{fungi}) or bacterial ($k_{bacteria}$) biomass (in per day); R represents the microbial respiration rate (in per day); f_{resp} is the fraction factor defining the proportion of C released as respiration during decomposition (unitless).

2.2 Representation of fungal- and bacterial-mediated processes by column

In the CLM-Microbe model, land surface heterogeneity was represented using a hierarchical data structure, which is adapted from CLM4.5. Each land grid cell can contain multiple land units (e.g., glacier, lake, wetland, urban, vegetated land, and cropland) and each land unit can be further divided into multiple soil/snow columns. On the vegetated land units, multiple (up to 16) plant functional types (PFTs) distinct in physiology and structure from different climate zones (e.g., needleleaf-evergreen-tree-boreal vs. needleleaf-deciduous-tree-boreal, broadleaf-evergreen-tree-tropical vs. broadleaf-deciduous-tree-tropical, and c3-arctic-grass vs. c3-non-arctic-grass) can occupy space on the column. All vegetation fluxes and state variables were defined at the PFT level, while soil fluxes and state variables were defined at the column level.

In the CLM4.5 and early versions of the CLM-Microbe model (before January 2021), parameters related to soil processes, such as decomposition, were assumed to be homogenous across data structure levels. Our previous work suggested the differences in microbial processes among biomes (He et al., 2021), the implicitly accounted sub-grid microbial processes may introduce uncertainties in the estimation of soil and microbial fluxes and state variables. Since soil flux and state variables in the CLM-Microbe model are defined at the column level, we represented the heterogeneity of microbe-mediated processes by column. Each PFT shares similar physical, phylogenetic and phenological characteristics, we thus assigned the parameter set of microbial properties by PFT. Furthermore, we determined the microbial properties of each column by the relative weight of PFTs occupied on the column, with the parameter set of the most dominant PFT adopted to represent the microbial and soil processes (e.g., fungal and bacterial biomass turnover rate, DOM degradation rate, and fungal and bacterial C assimilation proportion from SOM, litter, and DOM) on the column.

https://doi.org/10.5194/bg-2023-15
Preprint. Discussion started: 1 March 2023

2.3 Model forcing data

The forcing data for the CLM-Microbe model include meteorological variables such as air temperature, relative humidity, incoming solar radiation, longwave radiation, precipitation rate, surface pressure, and surface winds. In this study, we used the CRUNCEP dataset to force the CLM-Microbe model, which has been widely used to force the CLM. The CRUNCEP dataset is a combination of two existing datasets, i.e., the Climate Research Center timeseries (CRU TS) dataset of 0.5° × 0.5° at a monthly scale and the National Centers for Environmental Prediction (NCEP) reanalysis dataset of 2.5° × 2.5° at 6-hourly scale. In the CRUNCEP dataset, the diurnal and daily variation of variables such as the air temperature, precipitation, humidity, solar radiation, surface pressure, downward longwave radiation, and wind speed were derived from NCEP dataset, while their monthly means are bias corrected by the CRU TS dataset. In this study, the CRUNCEP dataset version 7, with a spatial resolution of 0.5° × 0.5°, spanning from 1901 to 2016, was used to drive the model simulation (Viovy, 2018). More information about the CRUNCEP dataset version 7 is available at https://rda.ucar.edu/datasets/ds314.3/.

In addition to the meteorological data, we forced the CLM-Microbe model using time-varying CO_2 concentration, N deposition, and aerosol concentration to estimate the C cycle change in the last century, provided by National Center for Atmospheric Research (NCAR) for forcing the CLM offline simulations. Atmospheric N deposition during 1849-2006 with a spatial resolution of 1.25° longitude × 0.9° latitude was applied for all simulations. The CO_2 concentrations remained fixed at 1850 levels (284.7 ppm) for accelerated decomposition and final runs and followed by transient historical (1849-2006) changes in the transient run. The aerosol concentration in accelerated decomposition and final runs for offline simulation was prescribed at 1850 level, while aerosol concentration with a spatial resolution of 1.25° longitude × 0.9° latitude during 1765-2005 was used in the transient simulation. The transient land use and land cover change during the historical period is based on the dataset of the UNH Transient Land Use and Land Cover Change Dataset Version 1 (LUHa.v1), covering the period of 1850-2005, which was produced by University of New Hampshire research group (Louise Chini, George Hurtt, Steve Frolking; https://luh.umd.edu/readme_LUHa_v1.shtml).

2.4 Model implementation

The model implementation was carried out in three stages, with the spatial resolution of the simulations being 2.5° longitude × 1.9° latitude. First, we ran the accelerated decomposition spin-up to allow the system to reach its steady state (Koven et al., 2013; Thornton & Rosenbloom, 2005). We set the model simulations to 1200 years for the accelerated decomposition phase. Then, we ran a final spin-up of 100 years to ensure the system was ready for transient simulations during 1850-2016. For the model years of 1850-1900 in transient simulations, we cycled atmospheric forcing during 1901-1910 of the CRUNCEP dataset version 7 to force

https://doi.org/10.5194/bg-2023-15
Preprint. Discussion started: 1 March 2023

the model. Then, we used the atmospheric data during 1901-2016 of the CRUNCEP dataset version 7 to drive the simulation between 1901 and 2016. The CLM-Microbe model was initially parameterized by biome, and the initial setting for microbial parameters was adopted from He et al. (2021).

185

2.5 Validation data

Several datasets were employed in this study for model validation. To produce realistic soil conditions in the CLM-Microbe model at the grid level, we used datasets of SOC in the top 1 m soil profile from the Harmonized World Soil Database (HWSD) at 0.05-degree spatial resolution archived at Oak Ridge National Laboratory (Wieder, 2014) and SOC in the top 30 cm from the Global 190 Soil Organic C Map (GSOCmap) version 1.5 at a spatial resolution of 1 km provided by Food and Agriculture Organization of the United Nations (FAO, 2018) to validate the SOC in the top 1 m and 30 cm of the CLM-Microbe model, respectively. To guarantee the reasonability of vegetation productivity, GPP and NPP of MODIS gridded datasets with a spatial resolution of 30 seconds during 2000-2015 were used to compare with the simulated GPP and NPP, respectively (Zhao et al., 2005). To reproduce the soil C emission flux, SR and HR from Global Gridded 1-km Annual Soil Respiration Database (SRDB) version 3 available at Oak 195 Ridge National Laboratory were used to validate SR and HR, respectively (Warner et al., 2019). For FBC and BBC in the top 30 cm, the dataset of FBC and BBC with a resolution of 0.5 degrees obtained from He et al. (2020) was used to validate FBC and BBC in the top 30 cm in the CLM-Microbe model, respectively. Microbial biomass C (MBC), the sum of FBC and BBC, in the top 1 m of the CLM-Microbe model outputs were compared with Xu et al. (2013) for accuracy. The DOC in 0-30 cm and 0-1 m with a resolution of 0.5 degrees derived from Guo et al. (2020) were used to compare with that in the top 30 cm and 1 m, respectively, 200 from the CLM-Microbe output for validation. More details about the datasets used for validation can be found in Table S2. Ten-year (2000-2009) averages of simulated soil, vegetation, and microbial variables from the CLM-Microbe output were calculated to compare with those from observed datasets previously described.

Although most processes in the CLM-Microbe model were adapted from the CLM4.5, the modification of microbe-mediated 205 decomposition cascades and microbial functional group-mediated methane cycle may reduce the applicability of default parameters in the CLM4.5, Therefore, we optimized the model parameters related to plant, soil, and microbial processes based on SOC in the top 30 cm from GSOCmap and that in the top 1 m from HWSD dataset, vegetation GPP and NPP from MODIS, SR, and HR from SRDB, FBC and BBC (0-30 cm) in He et al. (2020), MBC in Xu et al. (2013), and DOC (0-30 cm and 0-1 m) in Guo et al. (2020). We primarily focused on parameters related to plant photosynthesis (e.g., *flnr*), e-folding factor for decomposition (e.g., 210 *decomp_depth_efolding*) to match the reported GPP, NPP, and SOC in the top 0-30 cm and 1 m. To calibrate the model to fit the observed FBC, BBC, and DOC, we adjusted parameters related to soil microbial (*k_fungi* and *k_bacteria*) and DOC (*k_dom*)

https://doi.org/10.5194/bg-2023-15
Preprint. Discussion started: 1 March 2023

turnover, microbial C assimilation efficiency (*m_rf_s1m*, *m_rf_s2m*, *m_rf_s3m*, and *m_rf_s4m*), the proportion of C being released as respiration (*m_batm_f* and *m_fatm_f*), plant C allocation (froot_leaf), and the N concentration of plant tissues (*leafcn* and *frootcn*) to optimize the model simulations of FBC, BBC, MBC, DOC, SR, and HR.

To assess the efficacy of the CLM-Microbe model, the available soil and vegetation variables from the CLM4.5, including GPP, NPP, HR, SR, and SOC in the top 30 cm and 1 m, were adopted for comparison. The simulation results during 1850-2014 was forced using GSWP3v1 (Dirmeyer et al., 2006), with environmental changing factors including N deposition and rising CO_2 considered in the historical simulation. The GPP, NPP, HR, SR, and SOC in the top 30 cm and 1 m were provided by Climate Data Gateway at National Center for Atmospheric Research (NCAR). The GPP, NPP, HR, SR, and SOC in the top 30 cm and 1 m were from CLM land-only release; more details can be found at https://www.earthsystemgrid.org/dataset/ucar.cgd.ccsm4.CLM_LAND_ONLY.html. All variables were at a resolution of 0.9° latitude × 1.25° longitude. The temporal resolutions were different among variables; GPP, NPP, SR, and HR are of a monthly output, whereas SOC in 0-30 cm and 0-1 m are of yearly simulations. Ten-year (2000-2009) averages of the CLM4.5-simulated GPP, NPP, HR, SR, and SOC (0-30 cm and 0-1 m) were calculated to represent the long-term soil and vegetation status and for comparison with observed variables.

Since observational datasets and model simulations are of different resolutions and 0.5 degree is the most widely used, we used the function of linint2 in NCAR Command Language to interpolate those datasets and model outputs from their original resolutions to 0.5 degrees. To make the maps comparable, we used the *nibble* and *extracted by mask* functions provided by ArcGIS version 10.2 (ESRI, Redlands, California, USA) to make all maps consistent in geographical boundary and missing values.

2.6 Model evaluation

To evaluate the model performance in capturing the spatial variation in soil and vegetation variables, we compared GPP, NPP, HR, SR, FBC and BBC in the top 30 cm, MBC (0-1 m), and DOC and SOC (0-30 cm and 0-1 m) reported by the observational datasets and simulated averages of these variables during 2000-2009. Due to the non-normality of those variables, Spearman's rank correlation was used to evaluate the overall model performance for those variables. The Spearman's rank correlation coefficient (r_s), measuring the strength and direction of association between two ranked variables, was calculated following the equation as below,

$$r_s = \frac{cov(R(x),R(y))}{\sigma_{R(x)}\sigma_{R(y)}} \quad \text{equation (8)}$$

https://doi.org/10.5194/bg-2023-15
Preprint. Discussion started: 1 March 2023

where r_s is the Spearman's rank correlation coefficient; R(x) means the rankings of variable x; R(y) indicates the rankings of variable y; cov(R(x),R(y)) is the covariance of R(x) and R(y); $\sigma_{(R(x)}$ and $\sigma_{R(y)}$ are the standard deviations of the rankings of variable x and y, respectively.

2.7 Statistical analysis

Due to the non-normality of simulated and observed GPP, NPP, HR, SR, FBC and BBC in the top 30 cm, MBC (0-1 m), and DOC and SOC (0-30 cm and 0-1 m), we examined the agreement between variables simulated by the CLM-Microbe model or CLM4.5 and corresponding observed values at the grid level using Spearman's rank-order correlation. Such analyses were conducted using the function of *cor.test* with a method of *spearman* in "stats" package in R (R Core Team, 2013). The differences in soil, vegetation, litter, and microbial variables between decadal averages of 1901-1910 and 2007-2016 were examined using an independent t-test, conducted with the function of *t.test* in "stats" package in R (R Core Team, 2013) by continents and with the function of *ttest* in NCAR Command Language (https://www.ncl.ucar.edu) by grid.

To identify external environmental controls of soil, vegetation, litter, and microbial variables, we examined the correlations between vegetation productivity and mean annual temperature (MAT) and precipitation (MAP) and correlations of soil temperature (ST) and moisture (SM) with soil, litter, and microbial variables with respect to their area-weighted averages at the grid level from 1901 to 2016. Considering the consistent but stronger environmental influence on soil and microbial variables in the top 30 cm than in the top 1 m, only correlations between external environmental factors and soil and microbial variables in the top 1 m were assessed whether an association exists. The correlations between external environmental factors (e.g., MAP, MAT, SM, and ST) and annual averages of GPP, NPP, HR, SR, VegC, and FBC, BBC, DOC, SOC, and LitC in the top 1 m at the global level during 1901-2016 were estimated using the Pearson's correlation. These statistical analyses above were performed and relevant figures (Figs. 1-7, 10, and 14) were plotted using "graphics" (R Core Team, 2013) and "ggcorrplot" (Kassambara & Kassambara, 2019) packages in R.

To estimate the changing rate of GPP, NPP, HR, SR, FBC and BBC in the top 30 cm, FBC, BBC, DOC, LitC, and SOC in the top 1 m, and VegC during 1901-2016, we conducted linear regression models for these variables with time at the grid level, with the changing rate indicated by the slope of the regression model. In addition, correlations between environmental factors (e.g., MAT, MAP, ST, and SM) and vegetation, soil, litter, and microbial variables including GPP, NPP, HR, SR, VegC, and FBC, BBC, DOC, SOC, and LitC in the top 1 m at the grid level were estimated using Pearson's correlation. Such statistical analyses were performed

https://doi.org/10.5194/bg-2023-15
Preprint. Discussion started: 1 March 2023

using NCAR Command Language (https://www.ncl.ucar.edu). Relevant figures (Figs. 8-9, 11-13, and 15-16) were produced using Matlab version 2021b (The MathWorks, Inc.).

3 Results

3.1 Model validation and comparison with the CLM4.5

The CLM-Microbe produced comparable results with most observed data and performed comparable to or slightly better than the CLM4.5 with respect to the global C budget (Table 1), latitudinal trend (Figures 1 & 2), and individual grid (Figures 3 & 4). The CLM-Microbe model and the CLM4.5 overestimated the GPP by 15.7% and 7.3%, respectively (Table 1). However, NPP simulated by the CLM-Microbe model and the CLM4.5 was overestimated by 1.3% and underestimated by 8.1%, respectively. Similarly, SR was overestimated in both the CLM-Microbe model (15.6%) and the CLM4.5 (4.0%). HR in the CLM-Microbe model and the CLM4.5 was overestimated by 1.7% and underestimated by 4.4%, respectively. Both the CLM-Microbe model and the CLM4.5 underestimated SOC (0-30 cm), by 8.5% and 22.4%, respectively, while SOC (0-1 m) in the CLM-Microbe model and the CLM4.5 was overestimated by 32.4% and underestimated by 21.4%, respectively. The FBC, BBC, MBC, and DOC, only available in the CLM-Microbe model, were better predicted in the top 30 cm than 1 m. The simulated FBC, BBC, and DOC in the top 30 cm were underestimated by 3.3% and overestimated by 26.7% and 24.9%, respectively, while MBC and DOC in the top 1 m were overestimated by 69.5% and 75.0%, respectively.

The CLM-Microbe model can reasonably reproduce the latitudinal trends of vegetation, soil, and microbial variables, with the model performance varied among variables and along soil depth (Figure 1). The latitudinal trends of both GPP and NPP in the CLM-Microbe model agreed with observed data with a slight overestimation at northern latitudes and in equatorial regions, but NPP was slightly underestimated in the southern hemisphere (Figures 1a & 1b). Both HR and SR simulated by the CLM-Microbe model agreed well with observed data in the Southern Hemisphere but were overestimated in equatorial regions and at mid-high latitudes and underestimated at low latitudes in the Northern Hemisphere (Figures 1c & 1d). Similar latitudinal trends of HR and SR were also observed in the CLM4.5 simulation (Figures 2c-2d). Soil C pools showed similar latitudinal patterns across soil depths (Figures 1e-1k). Specifically, DOC (0-30 cm and 0-1 m) was overestimated in equatorial regions but underestimated in northern temperate regions (Figures 1e-1f). Meanwhile, the CLM-Microbe model produced an overestimation of SOC (0-30 cm and 0-1 m) in equatorial and northern high-latitude regions, but underestimation in northern mid-latitude regions (Figures 1g & 1h). As opposed to the CLM-Microbe model, the CLM4.5 consistently underestimated SOC (0-30 cm and 0-1 m) along latitudes, except for SOC (0-1 m) at latitudes of >60° N. Similarly, both FBC and BBC in the top 30 cm were overestimated in equatorial and at northern high latitudes but underestimated in northern mid-latitude regions (Figures 1i & 1j). Overall, FBC (0-30 cm) at

https://doi.org/10.5194/bg-2023-15
Preprint. Discussion started: 1 March 2023

300 southern latitudes was well predicted by the CLM-Microbe model, but BBC (0-30 cm) in that region was underestimated, while MBC (0-1 m) was overestimated across latitudinal gradients (Figure 1k).

At the grid scale, the CLM-Microbe model–simulated vegetation, soil, and microbial variables were significantly consistent with the observed values (P<0.05; Figure 3). The CLM4.5 also indicated significant consistency between simulated and observed
305 vegetation and soil variables (P<0.05; Figure 4). Overall, both the CLM-Microbe model and CLM4.5 performed better at simulating GPP and NPP, while soil and/or microbial variables were relatively worse reproduced. The CLM-Microbe model–simulated GPP (r_s=0.91) and NPP (r_s=0.86) were significantly and positively related to their observed values (Figures 3a & 3b). The GPP (r_s=0.88) and NPP (r_s=0.82) in the CLM4.5 were also significantly and positively associated with observed values (Figures 4a & 4b). The SR tended to be better predicted than HR in both the CLM-Microbe model (r_s=0.70 for SR vs. r_s=0.68 for
310 HR) and the CLM4.5 (r_s=0.68 for SR vs. r_s=0.64 for HR) (Figures 3c & 3d, Figures 4c & 4d). The DOC in 0-1 m (r_s=0.36) was slightly better reproduced than in 0-30 cm (r_s=0.34) in the CLM-Microbe model (Figures 3e & 3f), while both the CLM-Microbe model (r_s=0.68 for 0-30 cm vs. r_s=0.63 for 0-1 m) and CLM4.5 (r_s=0.63 for 0-30 cm vs. r_s=0.59 for 0-1 m) performed better at simulating SOC in the top 30 cm than in the top 1 m (Figures 3g & 3h, Figures 4e & 4f). Similarly, the CLM-Microbe model performed better in simulating FBC and BBC in the top 30 cm than MBC in the top 1 m (r_s=0.43) (Figures 3i - 3k). In addition,
315 BBC (r_s=0.53) was better reproduced than FBC (r_s=0.46) in the top 30 cm.

3.2 Carbon fluxes and pools associated with vegetation, litter, microbes, and soil

The GPP, NPP, HR, and SR displayed increasing trends from 1901 to 2016 (Figure 5), with different magnitudes among variables. By 2016, GPP (30 PgC yr^{-1}) increased about twice more than NPP (13 PgC yr^{-1}). Similarly, the increase of SR (25 PgC yr^{-1}) was
320 about twice that of HR (12 PgC yr^{-1}) from 1901. Their increasing rates showed variations with time. We observed a relatively modest increase in GPP (0.21 gC m^{-2} yr^{-2}), NPP (0.108 gC m^{-2} yr^{-2}), HR (0.09 gC m^{-2} yr^{-2}), and SR (0.18 gC m^{-2} yr^{-2}) during 1901-1980, whereas the increase in GPP (0.35 gC m^{-2} yr^{-2}), NPP (0.113 gC m^{-2} yr^{-2}), HR (0.12 gC m^{-2} yr^{-2}), and SR (0.3 gC m^{-2} yr^{-2}) were more rapid from 1981 to 2016.

325 Microbial, vegetation, litter, and soil C pools increased from 1901 to 2016 despite the year-to-year variability (Figure 6). The VegC, FBC and BBC in the top 30 cm, and FBC, BBC, DOC, SOC, and LitC in the top 1 m increased by about 37, 1.0, 0.4, 1.2, 0.7, 2.4, 34, and 4 PgC, respectively, from 1901 to 2016. However, the temporal trends of those variables varied during 1901-2016. The VegC and LitC and SOC in the top 1 m showed a steady increase during 1901-2016 (Figures 6f & 6h), while FBC (0-30 cm and 0-1 m) decreased (-0.003 gC m^{-2} yr^{-1} for 0-30 cm and -0.01 gC m^{-2} yr^{-1} for 0-1 m) from 1901 to 1940 and increased (0.016 gC m^{-2}

https://doi.org/10.5194/bg-2023-15
Preprint. Discussion started: 1 March 2023

330 yr^{-1} for 0-30 cm and 0.02 gC m^{-2} yr^{-1} for 0-1 m) after 1940 (Figures 6a & 6b). The BBC (0-30 cm and 0-1 m) exhibited little change during 1901-1940 but increased significantly (0.006 gC m^{-2} yr^{-1} for 0-30 cm and 0.009 gC m^{-2} yr^{-1} for 0-1 m) during 1941-2016 (Figures 6c & 6d). The DOC (0-1 m) slightly decreased from 1901 to 1920 (-0.008 gC m^{-2} yr^{-1}) but increased after 1920 (0.03 gC m^{-2} yr^{-1}) (Figure 6e).

335 During 1901-2016, the decadal average of soil C (4527 PgC for 1901-1910 and 4564 PgC for 2007-2016) was the largest C pool in the soil-vegetation-litter system, about 15 times of the sum of vegetation (193 PgC for 1901-1910 and 230 PgC for 2007-2016) and litter (63 PgC for 1901-1910 and 68 PgC for 2007-2016) C (Table 2). Soil, litter, and vegetation C significantly increased from 1901-1911 to 2007-2016 (P<0.05). However, the absolute increase in those C pools were different, with soil (37.0 PgC) and vegetation (37.1 PgC) increased to a larger extent than litter (5.1 PgC). Although soil and vegetation increased to a similar extent,
340 vegetation (19.2%) showed a larger relative increase than soil (0.8%) due to its smaller pool size. Despite the smallest absolute increase, litter (8.0%) increased more than soil with respect to relative values.

3.3 Spatial pattern of vegetation and soil carbon fluxes

Compared with 1901-1910, GPP, NPP, HR, and SR increased across latitudinal gradients in 2007-2016 (Figure 7). However, the
345 magnitude of the increase differed among latitudinal gradients. Specifically, increases in GPP, NPP, HR, and SR were larger and more prominent at northern latitudes and equatorial regions than at southern latitudes. The decadal averages of GPP, NPP, HR, and SR significantly increased across continents by 2007-2016 relative to 1901-1910 (P<0.05), but the magnitudes of increase and the decadal averages of those variables during 1901-1910 and 2007-2016 were distinct among continents (Table 3). The ranking of continents by GPP, NPP, HR, and SR was consistent between 1901-1910 and 2007-2016. Asia and South America had the
350 largest GPP, NPP, HR, and SR during both periods, followed by Africa, North America, and Europe, whereas Australia/Oceania had the smallest fluxes. The absolute increases of GPP, NPP, HR, and SR from 1901-1910 to 2007-2016 were the largest in Asia and South America, followed by Africa, North America, and Europe. Australia/Oceania witnessed the smallest absolute increases. Compared with the absolute changes, relative changes in GPP, NPP, HR, and SR were more similar across continents. Asia and Europe displayed the most distinguished relative changes. While North America, Africa, South America, and Australia/Oceania
355 showed relatively minor and comparable relative changes.

Across the globe, GPP, NPP, HR, and SR showed similar spatial patterns and evident increases from 1901-1910 to 2007-2016 in the east coast of North America, central and northern South America, central Africa, eastern Asia, and West Europe (Figures 8a & 8b, 8d & 8e, 8g & 8h, and 8j & 8k). The increases in those regions were statistically significant (P<0.05; Figures 8c, 8f, 8i, and

https://doi.org/10.5194/bg-2023-15
Preprint. Discussion started: 1 March 2023

8l). Correspondingly, we observed positive relative change in those regions from 1901-1910 to 2007-2016 (Figures 8c, 8f, 8i, and 8l). The relative change was mostly positive globally, with >6.25% in relative change commonly observed and most prominent changes (>50%) in eastern Asia, southern and central Europe, central Africa, central North America, and the east coast of South America. However, we also observed decreases in GPP, NPP, HR, and SR, with major negative relative changes found in the Middle East (>50%). In addition, we also found subtle negative relative changes in grids of northeast North America.

The GPP, NPP, HR, and SR displayed similar spatial patterns of changing rates (Figures 9a - 9d). We found significant and the largest positive changing rates of GPP, NPP, HR, and SR in the east coast of North America, central and northern South America, central Africa, eastern Asia, southern and central Europe, and island southeast Asia from 1901 to 2016 (P<0.05). In addition, we also found subtle but significant negative changing rates of GPP, NPP, HR, and SR in Greenland, South Asia, and the Sahara (P<0.05).

3.4 Spatial pattern of vegetation, litter, microbial, and soil carbon stocks

Similar to C fluxes, C pools in vegetation, soil, microbes, and litter increased across latitudinal gradients from 1901-1910 to 2007-2016 (Figure 10). Overall, FBC and BBC in the top 30 cm, FBC, BBC, DOC, SOC, and LitC in the top 1 m, and VegC showed a small but to different extents of increase across latitudinal gradients. Specifically, the increases were more prominent at northern high latitudes and equatorial regions than at other latitudes.

The FBC and BBC in the top 30 cm and FBC, BBC, DOC, and SOC in the top 1 m were distinct among continents (Table 3). The ranking of continents by their pool sizes was consistent between 1901-1910 and 2007-2016. Asia had the largest reservoirs of FBC (0-30 cm and 0-1 m) during both periods. North America had the second largest FBC (0-30 cm) during both periods, followed by South America, Africa, Europe, and Australia/Oceania. The BBC (0-30 cm) was the largest in Asia, followed by North and South America, during both periods. The BBC (0-30 cm) was the same in Europe and Africa during both periods. Australia/Oceania has the smallest and same BBC in the top 1 m during both periods. The BBC (0-1 m) was the largest in Asia, followed by South America, North America, Africa, and Europe, during both periods. While BBC (0-1 m) was the smallest and the same in Australia/Oceania during both periods. The DOC and SOC in the top 1 m were the largest in Asia during both periods. The DOC (0-1 m) was comparable between 1901-1910 and 2007-2016 in Europe and South America, but not SOC (0-1 m). The DOC and SOC in the top 1 m were the second smallest in Africa and the smallest in Australia/Oceania. Asia and South America had the largest ten-year averages of VegC and LitC (0-1 m) during both periods, followed by Africa, North America, and Europe. Such pools were the smallest in Australia/Oceania during both periods.

https://doi.org/10.5194/bg-2023-15
Preprint. Discussion started: 1 March 2023

390

The FBC and BBC in the top 30 cm and FBC, BBC, DOC, and SOC in the top 1 m significantly increased from 1901-1910 to 2007-2016 across continents (P<0.05; Table 3). However, we also found slight but significant decreases of FBC and BBC in the top 1 m and DOC (0-1 m) in Australia/Oceania (P<0.05). The absolute increase of FBC (0-30 cm and 0-1 m) were the largest in Asia and South America, followed by North America and Africa. The smallest absolute increase of FBC (0-30 cm) was observed
395 in Europe. Similarly, the absolute growth of BBC (0-30 cm and 0-1 m) was the largest in Asia and South America, followed by North America, Europe, and Africa. The absolute increases in DOC and SOC in the top 1 m were the largest in Asia. While the absolute increase in DOC (0-1 m) was the second largest in North America, followed by South America, Europe, and Africa, whereas that of SOC (0-1 m) in South America was the second largest, followed by Europe, Africa, and North America. Australia/Oceania had the smallest increase in SOC (0-1 m). The absolute increases of VegC and LitC (0-1 m) were the largest in
400 South America and Asia, followed by North America, Africa, and Europe, whereas Australia/Oceania witnessed the smallest absolute change of VegC and LitC (0-1 m).

In contrast to the absolute changes, the magnitude of relative changes in FBC and BBC in the top 30 cm and FBC, BBC, DOC, and SOC in the top 1 m were similar from 1901-1910 to 2007-2016 (Table 3). The most significant relative increases of FBC (0-
405 30 cm and 0-1 m) were in South America, whereas that of BBC (0-30 cm and 0-1 m) were in Europe. The second-largest relative change in FBC (0-1 m) was in Africa, while the second-largest relative change in BBC (0-30 cm and 0-1 m) was found in Africa and South America. Relative changes in FBC (0-30 cm) were comparable in Asia, North America, Europe, and Africa. Asia and North America were similar in the magnitude of relative changes in FBC (0-1 m) and BBC (0-30 cm and 0-1 m). The relative change in DOC (0-1 m) was most prominent in Europe and South America. Such changes were of a similar magnitude in Asia,
410 North America, and Africa, while the most remarkable relative increase of SOC (0-1 m) was in Africa, followed by Europe, South America, and Australia/Oceania. Such relative increases were comparable between Asia and North America for SOC (0-1 m). Relative changes in VegC and LitC (0-1 m) were to a similar extent. Europe displayed the largest relative changes in VegC and LitC (0-1 m), while Asia, North America, Africa, South America, and Australia/Oceania showed relatively smaller and comparable relative increases in VegC and LitC (0-1 m).

415

At the global scale, FBC and BBC in the top 30 cm and 1 m showed similar spatial patterns and widely increased from 1901-1910 to 2007-2016 (Figures 11a & 11b, 11d & 11e, 11g & 11h, and 11j & 11k). For example, we found higher increases of FBC and BBC in the top 30 cm and 1 m at northern high latitudes of Europe and Asia, central and northern South America, east coast of South America, and central Africa. In addition, such increases in those regions reached the statistical significance level (P<0.05;

https://doi.org/10.5194/bg-2023-15
Preprint. Discussion started: 1 March 2023

Figures 11c, 11f, 11i, and 11l). Correspondingly, we observed positive relative changes in FBC and BBC in the top 30 cm and 1 m in those regions from 1901-1910 to 2007-2016 (Figures 11c, 11f, 11i, and 11l). Similarly, positive relative changes in FBC and BBC in the top 30 cm and 1 m were widely observed across the globe, with the most prominent changes (>50%) in eastern Asia, central and northern Europe, and central North America. However, we also observed negative relative changes in FBC and BBC in the top 30 cm and 1 m. The largest relative decreases (>50%) were found in southern Europe and central North America. In addition, we also found grids with negative relative changes in FBC and BBC in the top 30 cm and 1 m in South Asia, southern Australia/Oceania, central Africa, and central South America.

Similarly, DOC (0-1 m) showed higher increases in central and northern Europe, east and northern Asia, east coast of South Africa, central and northern South America, and central and southern Africa from 1901-1910 to 2007-2016 (Figures 12a & 12b). Such increases in those regions were significant (P<0.05), and the relative changes in DOC (0-1 m) also suggested positive values in those regions from 1901-1910 to 2007-2016 (Figure 12c). Positive relative changes in DOC (0-1 m) were commonly found across the globe, with the most prominent changes (>50%) in eastern Asia, central and northern Europe, central North America, and the east coast of South America. However, we also observed negative relative changes in DOC (0-1 m) in South Asia, southern Europe, central and southern North America, southern Australia/Oceania, and central Africa. We also widely observed increases in SOC (0-1 m) by 2007-2016 relative to 1901-1910 (Figures 12d & 12e), which reached the significance level of 0.05 (Figure 12f). The highest relative increases were found in eastern Asia and central and northern South America, while South Asia displayed decreases in SOC (0-1 m) (Figure 12f). The VegC and LitC (0-1 m) exhibited similar spatial patterns and widely increased across the globe (Figures 12g - 12l). The most distinct and significant absolute increases of such variables were in west North America, eastern Asia, central and northern South America (P<0.05). The relative change in both VegC and LitC (0-1 m) were mostly positive across the globe, but the magnitudes were different. The most prominent relative increases of VegC and LitC in the top 1 m were in central Europe, eastern Asia, central and northern South America, and central North America. However, the relative change in VegC was to a larger extent than in LitC (0-1 m). Despite the widely increase, both VegC and LitC (0-1 m) decreased in South Asia.

The FBC and BBC in the top 30 cm, DOC, SOC, and LitC of top1 m, and VegC showed similar spatial patterns of changing rates (Figures 13a - 13h). Increasing temporal trends of such variables were widely observed across the globe, but weak decreasing trends were also found in Greenland, the Sahara, South Asia, and southern Australia/Oceania. However, the distribution of the fastest increasing rates was different among variables. Grids with significant and fastest increasing rates of FBC and BBC in the top 30 cm and 1 m were at northern latitudes of Northern America and Asia, eastern Asia, central and northern South America,

https://doi.org/10.5194/bg-2023-15
Preprint. Discussion started: 1 March 2023

and central Africa, and island southeast Asia (P<0.05; Figures 13a - 13d). Similarly, DOC in the top 1 m showed significant and the fastest increasing rates at northern latitudes of Northern America and Asia, eastern Asia, and some grids along the east coast of South America (P<0.05; Figure 13e). Spatial patterns of SOC and LitC in the top 1 m and VegC changing rates were similar (Figures 13f & 13h). The significant and fastest increasing rates of such variables were observed in the east coast of North America, central and northern Europe, eastern Asia, southeast Asia, central and northern South America, and central Africa (P<0.05).

3.5 Environmental controls on C cycling

The area-weighted average of GPP, NPP, and VegC were significantly correlated with those of MAT and MAP (P<0.05; Figure 14a). However, the correlations with MAT are stronger than with MAP. The area-weighted MAP and MAT had widely significant correlations with GPP, NPP, and VegC, and the spatial patterns of those correlations were similar among GPP, NPP, and VegC. However, the spatial patterns of correlations with MAT were different from those with MAP (Figure 15). The significant positive correlations of MAT with GPP, NPP, and VegC were found at middle and high latitudes of North America, Europe, and Asia, central Africa, the east coast of South America, and the southern edge of Asia, South America, and Australia/Oceania (P<0.05; Figures 15a, 15c, and 15e). In addition, we also found significant negative correlations of MAT with GPP, NPP, and VegC in southeast North America, South Asia, southern Africa, and central and northern Australia/Oceania (P<0.05). Despite the similar spatial pattern, there were differences in the strengths and signs of those correlations. For example, both GPP and VegC had significant positive correlations with MAT in northeast South America (P<0.05), while correlations between NPP and MAT were weak negative in such regions. The GPP and NPP showed significant negative correlations with MAT in northwest South America (P<0.05), but the correlation between MAT and VegC was weak (P>0.05). In addition, GPP and NPP showed significant positive correlations with MAT in central Africa (P<0.05), while the correlation between VegC and MAT was weak in that area (P>0.05).

Significant positive correlations of GPP, NPP, and VegC with MAP were also widely found (P<0.05; Figures 15b, 15d, and 15f). However, we also found weak negative correlations in the northern and east edge of Asia and central Africa. In addition, although correlations of MAP with GPP, NPP, and VegC were similar in spatial patterns, correlations with GPP and NPP tended to be stronger than with VegC. For example, strong (r>0.5) correlations of MAP with GPP and NPP were commonly observed across the globe, while the proportion of grids with strong correlations was to a lesser extent for VegC in central Australia/Oceania and southern Africa.

The area-weighted average of HR, SR, and FBC, BBC, DOC, SOC, and LitC in the top 1 m were significantly correlated with that of ST and SM in the top 1 m (P<0.05; Figure 14b). However, the strengths of correlations depended on both environmental controls

https://doi.org/10.5194/bg-2023-15
Preprint. Discussion started: 1 March 2023

(ST and SM) and variables (HR, SR, FBC, BBC, DOC, SOC, and LitC in the top 1 m). For example, correlations of HR and SR with ST and SM in the top 1 m were of the same magnitude, while the FBC, BBC, DOC, SOC, and LitC were more strongly correlated with ST than with SM in the top 1 m.

In contrast, soil, litter, and microbial variables were more widely and positively correlated with ST than with SM in the top 1 m (Figure 16). Correlations of ST (0-1 m) with HR and SR were similar in spatial pattern. We observed significant positive correlations of HR and SR with ST (0-1 m) at middle and high latitudes of North America, Europe, and Asia, central Africa, northeast South America, and the southern edge of Asia, South America, and Australia/Oceania (P<0.05; Figures 16a & 16c). While negative correlations of HR and SR with ST (0-1 m) were found in southwest Asia, southeast North America, central North America, central Africa, and central and northern Australia/Oceania. The FBC, BBC, DOC, and SOC in the top 1 m displayed similar spatial patterns (Figures 16e, 16g, 16i, and 16k). We found significant and positive correlations of FBC, BBC, DOC, and SOC with ST in the top 1 m at middle and high latitudes of North America, Europe, and Asia, central Africa, northeast South America, and the southern edge of Asia, South America, and Australia/Oceania (P<0.05). In addition, we also found some girds with negative correlations in central North America, Europe, Asia, South America, Africa, and Australia/Oceania. In contrast, correlations between LitC and ST in the top 1 m were equally found to be positive and negative (Figure 16m). Significant positive correlations were observed in central Europe and Asia, northeast South America, central and east coast of Africa, and southern and central Australia/Oceania; while significant negative correlations were distributed in northeast Asia (P<0.05).

Correlations of HR, SR, and FBC, BBC, DOC, and SOC with SM in the top 1 m were similar in spatial patterns, with significant and positive correlations observed at high latitudes in North America, Europe, and Asia, some grids of central Africa, and central and northern Australia/Oceania and negative correlations at middle and low latitudes in North America, Europe, and Asia, east coast of South America and Africa, and southern Australia/Oceania (P<0.05; Figures 16b, 16d, 16f, 16h, 16j, and 16l). In contrast, correlations between LitC and SM in the top 1 m were mostly negative, which reached the significance level of 0.05 at high latitudes of North America, Asia, and northwest Asia, southern and central Africa, and southern Australia/Oceania (P<0.05; Figure 16n). In addition, some grids with significant and positive correlation coefficients were scattered throughout central Africa, southwest Asia, and central and northern Australia/Oceania (P<0.05).

4 Discussion

4.1 Comparison with previous studies

https://doi.org/10.5194/bg-2023-15
Preprint. Discussion started: 1 March 2023

The latitudinal trends and grid-level distribution of GPP, NPP, HR, SR, FBC and BBC in the top 30 cm, and FBC, BBC, DOC, and SOC in the top 1 m were well-reproduced in the CLM-Microbe model (Figures 1 & 3). The CLM-Microbe model performed better than or comparable to the CLM4.5 in simulating the spatial distribution of vegetation, soil, and microbial variables (Figures 2 & 4). In line with our results, multiple ESM models captured the spatial variation of GPP, NPP, HR, and SR (Delire et al., 2020; Kim et al., 2019; Wiltshire et al., 2021; Zheng et al., 2020). Wieder et al. (2015) reported a high spatial correlation (r = 0.46) of SOC (0-1 m) between MIMICS outputs and HWSD. In addition, Wang et al. (2017) observed the high consistency in SOC (0-1 m) (R^2=0.96; P<0.01) between the TRIPLEX-MICROBE model and HWSD by vegetation type. The well-developed plant physiology and environmental controls in the model may explain the good performance of ESMs in simulating vegetation and soil processes (Flato, 2011; Mathieu & O'Neill, 2008). However, the latitudinal trends and grid-level distribution of DOC, SOC, and MBC (sum of FBC and BBC) in the top 1 m were relatively worse reproduced than those in the top 30 cm (subfigures e-k of Figures 1 & 3, subfigures e-f of Figures 2 & 4), indicating that the vertical distribution of processes related to decomposition, microbial turnover, and plant C input needs further improvements. Although parameters classifying the active decomposition depth and biological function to perturbation were defined in the CLM-Microbe model, the gradual change of microbial turnover and activity defined along soil profile may need to be improved in future models (Preusser et al., 2019; Zhu et al., 2021). In addition, processes or parameters related to the active layer for decomposition and perturbation caused by biological (e.g., nematode) and abiotic (e.g., drying and rewetting) activities can cause uncertainties in the vertical distribution of C cycle, which needs further efforts and attention in model development (Ettema & Wardle, 2002; Gabet et al., 2003; Kuzyakov & Blagodatskaya, 2015; Schimel, 2018).

We estimated global annual averages of 129.5, 56.5, 99.8, and 49.8 PgC yr^{-1} for GPP, NPP, HR, and SR, respectively (Table 1). Consistent with our results, previous studies reported similar values of GPP, NPP, HR, and SR (Cramer et al., 1999; Hashimoto et al., 2015; Huang et al., 2020; Lu et al., 2021; Nemani et al., 2003; Zhao et al., 2017; Zheng et al., 2020). The consistent simulations and reasonable estimations of GPP, NPP, HR, and SR across models may indicate the convergent plant physiology among models, and well-defined soil and microbial processes in the CLM-Microbe model. In addition, compared with observed data, the CLM-Microbe model produced more consistent NPP and HR but overestimated GPP and SR (Table 1). The overestimation of GPP and SR may be due to the lower ecosystem-scale C use efficiency (CUE) in the CLM-Microbe model. The vegetation physiology module in the CLM-Microbe model is adapted from CLM4.5. The ecosystem-scale CUEs between the CLM-Microbe model (0.44) and CLM4.5 (0.43) were comparable but lower than in MODIS (0.5). Correspondingly, we observed a higher contribution of roots to total SR in the CLM-Microbe model (0.5) and the CLM4.5 (0.48) than in the observed SRDB dataset (0.43). Therefore, the well-simulated NPP and HR but higher predicted GPP and SR in the CLM-Microbe model were attributed to the low ecosystem-

https://doi.org/10.5194/bg-2023-15
Preprint. Discussion started: 1 March 2023

scale CUE in the CLM-Microbe. Increasing ecosystem-scale CUE in the CLM-Microbe model will improve the modeling performance of GPP and SR in model development.

The CLM-Microbe model can reasonably predict FBC, BBC, and DOC in the top 30 cm well at the global level, indicating the well-represented microbial processes in surface soils (Table 1). However, MBC and DOC in the top 1 m were vastly overestimated, with MBC and DOC in the top 1 m overestimated by 69.5% and 75.0%, respectively. Inconsistent with our results, previous studies suggested the underestimation of MBC (0-1 m). For example, Wang et al. (2017) estimated the global MBC as 21 PgC in the TRIPLEX-MICROBE model. Wieder et al. (2015) suggested the steady-state MBC (0-1 m) of 16.3 Pg in the MIMICS. The relatively poor performance of the CLM-Microbe model in simulating DOC and MBC in the top 1 m and the discrepancy in simulated MBC (0-1 m) among studies may result from three aspects. First, the active layer in the CLM-Microbe model may not be sufficient to define soil microbial processes along soil profile. We observed better performance of the CLM-Microbe model in simulating FBC, BBC, and DOC in the top 30 cm relative to MBC and DOC in the top 1 m, indicating that the representation of microbial and soil processes along soil profile may need improvements. Second, the difference in calibration for MBC may cause discrepancy between studies. The SOC in Wieder et al. (2015) was calibrated to observed data but not MBC, Wang et al. (2017) calibrated the MBC (0-1 m) in the TRIPLEX-MICROBE by vegetation types, while we calibrated both MBC and SOC in 0-30 cm and 0-1 m by grid in the CLM-Microbe model. The differences in variables and depths calibrated between studies can partly explain the discrepancy. Third, the difference in simulated vegetation, litter, and soil C pools among studies can result in the discrepancy. Vegetation C as litter and volatile C input, DOC, and SOC are the C source for microbial C assimilation through decomposition (Figure S1). Consequently, the overestimation of SOC and DOC can partly explain the overestimation of MBC in the top 1 m (Table 1).

The CLM-Microbe model suggested pool sizes of 605 PgC in 0-30 cm and 1631 PgC in 0-1 m, indicating an underestimation of 8.5% for SOC (0-30 cm) and an overestimation of 32.4% for SOC (0-1 m) when comparing with observed data (Table 1). Compared with the CLM4.5, the CLM-Microbe predicted larger stocks of SOC (0-30 cm and 0-1 m). Previous studies suggest large variations in simulated SOC (0-1 m) among models. For example, Todd-Brown et al. (2013) reported the SOC (0-1 m) stock ranging from 510 to 3040 PgC among 11 CMIP5 ESMs. The TRIPLEX-MICROBE modeled the global SOC (0-1 m) stock as 1195 PgC (Wang et al., 2017). Wieder et al. (2015) documented the steady-state SOC pool in the MIMICS as 1530 PgC. Delire et al. (2020) reported the SOC (0-1 m) as 1611 PgC and 1520 PgC in the new (ISBA_bgc6) and old (ISBA_bgc5) versions, respectively, of ISBA-CTRIP. Given the wide range (510 to 3040 PgC) of simulated SOC (0-1 m) in models, the CLM-Microbe model thus predicted reasonable SOC stocks.

https://doi.org/10.5194/bg-2023-15
Preprint. Discussion started: 1 March 2023

570 **4.2 Temporal trends of carbon fluxes and stocks**

The area-weighted average of GPP, NPP, HR, and SR in the CLM-Microbe model increased by 30, 13, 12, and 25 PgC yr^{-1}, respectively, from 1901 to 2016 (Figure 5). Consistent with our findings, Wiltshire et al. (2021) also observed the increasing trends of GPP and NPP in the JULES model, with GPP and NPP increased by about 12 and 25 PgC yr^{-1}, respectively, from 1901 to 2005. Bonan et al. (2019) observed the increase of about 20 PgC yr^{-1} of GPP, 10 PgC yr^{-1} of NPP, and 8 PgC yr^{-1} of HR from 1850 to
575 2014 in the CLM4.5. The global increasing rate of SR was estimated as 0.04-0.14 PgC yr^{-1} by Huang et al. (2020). Temperature, water, CO_2 concentration, and N are key factors determining plant photosynthesis, the increasing N deposition and rising CO_2 concentration and temperature may explain the enhancement of vegetation productivity under environmental change (Dusenge et al., 2019; Piñeiro et al., 2017). In this study, we observed significant and positive correlations of GPP and NPP with MAT and MAP (Fig. S2a). Although the compounding effects of such environmental change factors also have positive effects on autotrophic
580 respiration, but to a lesser extent, leading to increasing vegetation productivity in terrestrial ecosystems (Delire et al., 2020). In addition, the rising ST (0-1 m) may explain the observed increase in HR considering the positive relationship between ST (0-1 m) and HR (Figures 14 & S2b). The increase of HR can partly explain the rising SR from 1901 to 2016 given its critical contribution to SR. In addition to HR, the increase in root respiration due to increasing C availability and rising temperature accounted for a crucial proportion of the SR increase (Bond-Lamberty & Thomson, 2010; Hashimoto et al., 2015; Piñeiro et al., 2017; Zhou et al.,
585 2016). Therefore, the increase of GPP and NPP can be associated with environmental change (e.g., rising MAP and MAT). Increases of GPP and NPP together with rising ST and SM in top 1 m enhanced HR and SR in the last century. Similar with GPP and NPP, by 2007-2016, both LitC (0-1 m) (4 PgC) and VegC (37 PgC) increased (Fig. 6g-h), which is consistent with a previous study (Bonan et al., 2019). The VegC indicates the C stock of vegetation biomass, while LitC is the C loss of vegetation biomass. Increasing water availability and temperature usually have negative impacts on maintenance of vegetation biomass and litter in the
590 soil (Delire et al., 2020), while we observed positive correlations of VegC with MAT and MAP and of LitC with SM and ST in the top 1 m (Fig. 14). Therefore, the increase of LitC (0-1 m) and VegC may attributed to increases in GPP and NPP in the last century.

The area-weighted FBC and BBC in 0-30 cm increased by 1.0 and 0.4 PgC and those in 0-1 m increased by 1.2 and 0.7 PgC,
595 respectively, from 1901 to 2016 in the CLM-Microbe model (Figures 6a & 6d). In addition, both DOC (2.4 PgC) and SOC (34 PgC) in the top 1 m increased from 1901 to 2016 (Figures 6e & 6f). Similarly, Bonan et al. (2019) also observed the increase of SOC (0-1 m) by about 30 PgC from 1850 to 2014 in the CLM4.5. Rising temperature has negative impacts on fungal and bacterial biomass due to its facilitating effects on microbial turnover (He & Xu, 2021). Meanwhile, the observed increase in FBC and BBC

https://doi.org/10.5194/bg-2023-15
Preprint. Discussion started: 1 March 2023

in the top 30 cm and 1 m in the CLM-Microbe model, indicating the higher decomposition potential of soil microbial community (Figure S1). In addition, rising temperature and water availability promotes microbial decomposition (Allison et al., 2010; Qiu et al., 2005; Wardle & Parkinson, 1990). Despite those negative impacts on microbial biomass maintenance and SOC stabilization, we observed increases in microbial and soil C pools from 1901 to 2016. Vegetation provides the major C source for microbial C assimilation and soil C sequestration, increases in GPP and NPP can explain the increasing trends of soil and microbial C pools during 1901-2016. Litter, SOM, and DOC are three C sources for soil microbes in the CLM-Microbe model (Materials and methods; Figure S1). The positive temporal trends of DOC, LitC, and SOC can explain the increase in FBC and BBC in the CLM-Microbe model (Figure 6).

The annual averages of fluxes (GPP, NPP, HR, and SR) and pools (FBC, BBC, DOC, LitC, and SOC in the top 1 m and VegC) exhibited more rapid increases since 1980 (Figures 5 & 6). Concurrently, we observed a more rapid increase in MAT, MAP, and ST and SM in the top 1 m since 1980 (Figure S2). In line with this study, Cheng et al. (2017) analyzed SM simulations during historical (1920–2005) and future (2006–2080) periods in the CESM from CIMP5; they also found 1980 as a transition for a subsequent increase of variation during 1920-2005, indicating more rapid changes in SM after 1980. We observed significant correlations of GPP, NPP, and VegC with MAT and MAP (Figure 14a) and of HR, SR, and FBC, BBC, DOC, LitC, and SOC with ST and SM in the top 1 m (Figure 14b). Therefore, more rapid increases in MAT, MAP, and ST and SM in the top 1 m after 1980 may explain the more rapid increases of such variables since 1980.

4.3 Changes in carbon fluxes and stocks over the space and their controls

The GPP and NPP increased across latitudinal gradients and continents from 1901-1910 to 2007-2016 (Figures 7a & 7b, Table 3; Figures 8a - 8f, 9a & 9b). Across the globe, absolute increases of GPP and NPP were the largest in Asia (particularly eastern Asia) and South America (particularly central and northern South America), while relative increases of GPP and NPP were the largest in Asia (particularly eastern Asia) and Europe (particularly southern Europe) (Table 3; Figures 8a - 8f, Figures 9a & 9b). Their largest increases in GPP and NPP were evidenced by the fastest-increasing rates of GPP and NPP in those areas (Figures 9a & 9b). The grids with fast-increasing rates of GPP and NPP and the higher number of such grids as well as their relatively large land areas (44.6 million km² for Asia and 17.7 million km² for South America vs. 24.6 million km² for North America, 9.8 million km² for Europe, 29.9 million km² for Africa, and 8.1 million km² for Australia/Oceania) were responsible for the largest absolute increase of GPP and NPP in Asia and South America. While grids with fast-increasing rates of GPP and NPP and the higher proportion of such grids can explain the largest relative increase of GPP and NPP in Asia and Europe. In line with this study, Zheng et al. (2020) reported that GPP in vegetated areas, particularly temperate and humid regions (e.g., most of Asia and central and southern Africa),

https://doi.org/10.5194/bg-2023-15
Preprint. Discussion started: 1 March 2023

increased from 1982 to 2017 in the revised EC-LUE model. Yue et al. (2015) observed distinguishing increases in GPP and NPP in central Africa, the Amazon, Europe, eastern Asia, and North America in the YIBs model. The broad increase in vegetation productivity may be due to the positive effects of elevated CO_2 and N deposition (Zheng et al., 2020). In addition, temperature and water availability have a profound influence on plant growth and land C fluxes (Yue et al., 2015; Zheng et al., 2020). Our results showed significant correlations of GPP and NPP with MAT and MAP (Figures 15a - 15d). The wide increase in MAP and MAT can partly explain the increase in GPP and NPP along latitudes and over continents (Figure S3). Large increases in eastern Asia, central and northern South America, and southern Europe may be related to changes in MAT and MAP, considering their significant correlations from 1901-1910 to 2007-2016 (Figures S3a & S3b). Given the significant positive correlations of GPP and NPP with MAT and MAP in southern Europe, the large relative increase of GPP and NPP may be associated with the increasing MAT and MAP in that area. However, correlations of GPP and NPP with MAT and MAP varied with latitude in Asia, correlations of GPP and NPP with MAT and MAP were significant and positive at middle and high latitudes, but negative at low latitudes. Therefore, increases in GPP and NPP at middle and high latitudes may be related to rising MAT and those at low latitudes were associated with decreasing MAP. In central and northern South America, correlations between GPP and NPP and MAT and MAP were complex. Correlations of GPP and NPP with MAT were not consistent in such areas, while GPP and NPP were consistently and positively correlated with MAP in central and northern South America. As a result, the increase of GPP and NPP in central and northern South America may be related to the increasing MAP. In addition, we also observed decreases in GPP and NPP in the Middle East (Figures 8a-8f). The decreases in GPP and NPP can be explained by the increases in MAT and decreases in MAP (Figures 15a - 15d). In contrast to the increasing trend of GPP in Amazon region during 1982-2016 in this study (~+5 gC m^{-2} yr^{-2} for most grids; P<0.05), Zheng et al. (2020) observed decreased GPP in tropical regions such as the Amazon Forest from 1982 to 2017 using the revised EC-LUE model. In addition to CO_2, N deposition, and meteorology, vegetation cover and type play an important role on GPP (Zheng et al., 2020). Land use and land cover change due to management practices have substantial effects on plant growth; such effects on leaf area index were considered in the revised EC-LUE model but not in our simulation. Therefore, the discrepancy between studies may be caused by land-use effects.

The HR and SR showed a wide increase from 1901-1910 to 2007-2016 along latitude, across the globe, and over continents (Table 3; Figures 7c & 7d, 8k & 8l, 9c & 9d). Consistent with our findings, Huang et al. (2020) observed a globally significant increase in SR, particularly in boreal and tropical regions (e.g., northern Asia, central South America, and central and southern Africa), from 2000 to 2014. Bond-Lamberty et al. (2018) also observed an increase of HR in multiple biomes during 2000-2015. In addition, we observed the largest absolute increase of HR and SR in Asia and South America (e.g., eastern Asia and central and northern South America) and the largest relatively increase in Asia and Europe (e.g., eastern Asia and southern and central Europe) at the

https://doi.org/10.5194/bg-2023-15
Preprint. Discussion started: 1 March 2023

continental scale, which was similar with GPP and NPP (Table 3; Figures 8k & 8l, 9c & 9d). These results indicated that soil C fluxes were largely dependent on vegetation productivity which can enhance soil C fluxes due to high C allocation to belowground (Pendall et al., 2004; Prescott et al., 2020). In addition, soil C fluxes can be further increased due to facilitated decomposition in a warming world (Noh et al., 2017; Zhou et al., 2007). Temperature and water availability have a profound influence on root respiration and HR (Bond-Lamberty & Thomson, 2010; Hashimoto et al., 2015; Sinsabaugh et al., 2016). We also found significant correlations of HR and SR with ST and SM in the top 1 m (Figures 16a - 16d). The large increases in eastern Asia, central and northern South America, and southern and central Europe may be related to changes in SM and ST in the top 1 m considering their significant correlations (Figures S3c & S3d). Given the significant positive correlations of HR and SR with ST (0-1 m) and negative correlations of HR and SR with SM (0-1 m) in southern and central Europe, the increases in HR and SR were related to the rising ST and decreasing SM in the top 1 m in that area. However, correlations of HR and SR with ST (0-1 m) varied with latitude in eastern Asia, with significant positive correlations of HR and SR with ST and SM in the top 1 m at middle and high latitudes but negative correlations at low latitudes of eastern Asia. Therefore, increases in HR and SR at middle and high latitudes may be related to rising ST (0-1 m) and those at low latitudes were associated with decreasing SM (0-1 m). In central and northern South America, correlations of HR and SR with ST (0-1 m) were complex. The HR and SR were positively correlated to ST (0-1 m) in the east part, but negative correlations with SM (0-1 m) in central and northern South America. As a result, the increase of HR and SR in central and northern South America was associated with decreasing SM (0-1 m) and increasing ST (0-1 m). In addition, we also observed decreases of HR and SR in the Middle East (Fig. 8c-d). The decreases of GPP and NPP in such regions can explain the decrease in HR and SR (Figures 8a - 8f).

The VegC and LitC (0-1 m) also increased across latitudinal gradients and the globe by 2007-2016 relative to 1901-1910 (Figures 10g & 10h, 12g - 12l). Over continents, the absolute increase of VegC and LitC (0-1 m) was largest in Asia (e.g., eastern Asia) and South America (e.g., central and northern South America), where the relative increase was most distinct in Europe (e.g., southern and central Europe) (Table 3; Figures 13g - 13l). The VegC and LitC are closely related to vegetation biomass production, which partly explains the similar spatial patterns of VegC and LitC (top 1 m) with those of GPP and NPP. In addition, VegC and LitC (0-1 m) are affected by environmental factors such as temperature and water availability. We found significant correlations of VegC with MAT and MAP (Figures 15e & 15f) and LitC with ST and SM in the top 1 m (Figures 16m & 16n). Similar with GPP and NPP, the increase of VegC may be associated with the increasing MAT and MAP in southern and central Europe, increases of VegC at middle and high latitudes may be related to rising MAT and those at low latitudes may be associated with decreasing MAP in eastern Asia, while the increase of VegC in central and northern South America may be related to the increasing MAP. We observed significant negative correlations between SM and LitC in the top 1 m in eastern Asia, southern and central

https://doi.org/10.5194/bg-2023-15
Preprint. Discussion started: 1 March 2023

Europe, and central and northern South America (Figures 16m & 16n). The LitC and ST in the top 1 m were weakly and negatively correlated in southern and central Europe, significantly and positively correlated in east parts but weakly and negatively correlated in rest areas of central and northern South America, and weakly correlated in southern Europe. The temperature has positive impact on decomposition processes, leading to a decrease in litter residue (Pendall et al., 2004; Pietikäinen et al., 2005; Qiu et al., 2005). Therefore, increasing LitC in the top 1 m in eastern Asia and in southern and central Europe was related to their increased GPP, NPP, and VegC, while increases in LitC at low latitudes of eastern Asia and in southern and central Europe may be associated with the decreasing SM in the top 1 m.

The DOC and SOC in the top 1 m also increased across latitude by 2007-2016 relative to 1901-1910 (Figures 10e & 10f). In addition, DOC and SOC in the top 1 m widely increased over continents, with the most prominent absolute increase in Asia (e.g., eastern Asia) and relative changes in DOC in Europe (e.g., central and northern Europe) and South America (e.g., east coast of South America) and of SOC in Africa (e.g., central Africa), but slight decreases of DOC (0-1 m) were found in Australia/Oceania (southern Australia/Oceania) (Table 3; Figures 12a - 12c, 13e - 13f). In line with our results, Eglin et al. (2010) also recorded increasing soil C stock in Asia and South America in response to the combined effects of atmospheric CO_2 concentration and climate simulated by ORCHIDEE–LUC from 1901 to 2002. As vegetation C input provides the major C source for SOC stabilization, the large increases in GPP, NPP, VegC, and LitC (0-1 m) in eastern Asia may partly explain the large absolute increase of SOC in those regions (Figures 8a -f 8, 12g - 12l, 9a & 9b, 13g & 13h). The changes in environmental conditions can also affect SOC stock. Significant correlations of SOC with ST and SM in the top 1 m were observed (Figures 16k & 16l). We found significant and positive correlations between ST and SOC in central and southern Africa and at middle and high latitudes of eastern Asia and between SM and SOC at low latitudes of eastern Asia, while a significant and negative correlation between SM and SOC at low latitudes of eastern Asia were documented in the top 1 m. Since rising temperature exerts negative impacts on SOC stabilization, the increasing SOC in Africa, eastern Asia, and central Africa was associated with the increasing C input from vegetation, while increasing SOC at low latitudes of eastern Asia was also related to rising SM in the top 1 m (Figures 9a & 9b, 16k & 16l). However, contrary to our result, Eglin et al. (2010) found a slight decrease in soil C stock in Africa from 1901 to 2002. The SOC decline in Africa may be due to the missing temporal dynamics of N deposition in the ORCHIDEE–LUC. N has important impacts on plant growth and vegetation productivity and SOC formation, especially in N-limited areas such as arid and semiarid area in most African regions (Piñeiro et al., 2017). The DOC is the balance among SOC and litter decomposition, microbial lysis, and DOC degradation (Figure S1). The large increase of GPP, NPP, VegC, and LitC and SOC in the top 1 m in Asia, South America, and Europe can explain the increase of DOC (0-1 m) in those regions (Table 1; Figures 7a & 7b, 10f - 10h, 8a - 8f, 12d - 12l, 9a & 9b, 13f - 13h). In addition, we observed significant and positive correlations between DOC and ST in the top 1 m in

https://doi.org/10.5194/bg-2023-15
Preprint. Discussion started: 1 March 2023

eastern Asia, central and northern Europe, and the east coast of South America. Significant and positive correlations between DOC and SM in the top 1 m were observed in central and northern Europe and eastern Asia, while significant and negative correlations between DOC and SM in the top 1 m were observed at low latitudes of eastern Asia and along the east coast of South America. Therefore, increasing DOC in Europe, South America, and eastern Asia was partly due to increasing C input from litter and SOC decomposition, while increases in DOC at low latitudes of eastern Asia and along the east coast of South America were also related to decreasing SM in the top 1 m.

The FBC and BBC in the top 30 cm and 1 m increased across latitudes during 2007-2016 compared with 1901-1910 (Figures 10a - 10d). The FBC and BBC in the top 30 cm and 1 m widely increased at the continental level, with the absolute increase largest in Asia (e.g., eastern Asia) and South America (e.g., central and northern South America) for FBC and BBC in the top 30 cm and 1 m and relative increase largest in South America (e.g., central and northern and east coast of South America) for FBC (0-30 cm and 0-1 m) and in Europe (e.g., central and northern Europe) for BBC (0-30 cm and 0-1 m). Vegetation is the major C source for soil microbes in terrestrial ecosystems, determining the total amount of C available for microbes by regulating microbial C assimilation through SOC, DOC, and litter (Schimel, 1995; Vance & Chapin, 2001; Xu et al., 2014). This large increase of GPP and NPP in eastern Asia and central and northern South America could explain the largest absolute increase of FBC and BBC in top 30 cm and 1 m in such areas. However, fungi and bacteria have different preferences in using those C sources, with fungi generally better at using recalcitrant C (e.g., SOC) and bacteria generally preferring labile C (e.g., DOC). The fast-increasing rate of SOC in South America and DOC in Europe can partly explain the highest relative change of BBC (0-30 cm and 0-1 m) in Europe and FBC (0-30 cm and 0-1 m) in South America (Figures 13e & 13f). Moreover, the microbial biomass is closely associated with environmental factors, which highly impacts microbial processes such as lysis. Microbial turnover is negatively affected by rising temperature, with bacteria more affected than fungi due to the faster turnover rate of bacteria than fungi (He & Xu, 2021; Rousk & Bååth, 2011). The high air and soil temperature on central and northern and east coasts of Southern America may cause a faster turnover of bacteria than fungi, leading to a faster increase of bacteria in northern Europe and fungi in central and northern and east coasts of South America. However, we also found slight decreases of FBC and BBC in the top 1 m in Australia/Oceania (e.g., southern Australia/Oceania) (Table 3; Figures 11, 13a - 13d). The decrease of DOC (0-1 m) may explain the widespread decrease of FBC and BBC of 30 cm and 1 m in southern Australia/Oceania (Figures 11, 13a - 13d). Meanwhile, in the top 1 m, FBC and BBC were negatively correlated with ST and positively correlated to SM in southern Australia/Oceania (Figures 16e - 16h). The increase of ST and SM in the top 1 m can explain the decrease of FBC and BBC in 0-30 cm and 0-1 m in southern Australia/Oceania (Figures S3c & S3d).

https://doi.org/10.5194/bg-2023-15
Preprint. Discussion started: 1 March 2023

4.4 Future improvements

Although the CLM-Microbe model can well reproduce the global distribution of C in vegetation, soil, and microbes, four key improvements are identified for future work. First, soil and microbial processes along soil profiles need to be better defined. Soil and microbial variables such as DOC, SOC, FBC, and BBC in 0-30 cm were better simulated than those in 0-1 m (Table 1; Figures 1-3), indicating that soil and microbial processes along soil profile may not that well be represented in the current model version. Therefore, better defining soil and microbial processes along soil profile can help improve the model efficacy in capturing soil and microbial processes, and further reduce uncertainties in future projections of the C cycle. Second, land-use change needs to be considered in future work. In addition to meteorology, N deposition, aerosol, and elevated CO_2, land-use change also has profound influences on the plant, soil, and microbial processes. Drastic changes in vegetation, soil, and microbial processes due to land-use change can occur at small scales, and the spatial pattern of those processes can also be changed (Pascual et al., 1997; Sampaio et al., 2007; Stevenson et al., 2016). Therefore, considering the impacts of land-use change in the CLM-Microbe model can help improve the model efficiency in capturing spatial patterns of C density and stocks in terrestrial ecosystems. The global biogeographic patterns of soil microbes and their functions have been recognized (Xu et al., 2020), this modeling study has made progress toward a full investigation of microbial patterns and mechanisms, and a community-wide microbial data system is needed to facilitate more data-model integration to improve microbial models. Lastly, factorial analysis to attribute the variations in terrestrial C fluxes will be addressed in our future work. Variations in terrestrial C fluxes and pools are driven by multiple environmental change factors that contribute individually or in combination, attributing the variations in terrestrial C fluxes and pools to environmental change factors is important for the understanding of terrestrial C fluxes and pools dynamics (Xu et al., 2010).

5 Conclusion

The ESMs incorporating microbial processes are expected to represent uncertainties in the terrestrial C cycle more comprehensively. The CLM-Microbe model can well reproduce the distribution of vegetation (GPP, NPP, LitC, and VegC), soil (HR, SR, DOC, and SOC), and microbial (FBC, BBC, and MBC) variables. In addition, fluxes (GPP and NPP) and pools (HR, SR, FBC and BBC in top 30 cm, FBC, BBC, DOC, SOC, and LitC in the top 1 m, and VegC) increased from 1901 to 2016. We generally observed the largest absolute increases of such variables in Asia and South America, particularly in eastern Asia and central and northern South America. While relative increases of such variables varied over continents, with the largest relative increases of GPP, NPP, HR, and SR in Asia and Europe (particularly eastern Asia and southern and central Europe), FBC (0-30 cm and 0-1 m) in South America (particularly central and east coast of South America), BBC (0-30 cm and 0-1 m) in Europe (particularly central and northern Europe), DOC (0-1 m) in South America and Europe (particularly east coast of South America

and northern Europe), SOC (0-1 m) in Africa (particularly central and southern Africa), and VegC and LitC (0-1 m) in Europe (particularly southern and central Europe). Slight decreases of FBC, BBC, and DOC in the top 1 m in Australia/Oceania were also observed. The increase in GPP, NPP, and VegC were significantly related to rising MAT and MAP, while increases in FBC and BBC in top 30 cm and FBC, BBC, DOC, SOC, and LitC in the top 1 m were closely associated with increasing C input from vegetation and SM and ST in the top 1 m.

This study represents one of the first attempts to simulate the spatial and temporal variations C fluxes and pool sizes of soil, vegetation, litter, and soil microbes during the last century using a microbial-explicit model - the CLM-Microbe model. As the community is moving towards a microbial-explicit Earth system model, this study provides a robust support for microbial model development and application for predicting microbial roles in the C-climate feedback. The variations in soil microbial community over historical periods and across space simulated by the CLM-Microbe model provide a crucial foundation to study the impacts of soil microbes on terrestrial biogeochemical processes.

Acknowledgments

This study has been supported by an NSF CAREER project (2145130), an NSF RAPID award (2154746), and the CSU Program for Education & Research in Biotechnology. Support for this work for M.A.M. was provided by an Early Career Award through the U.S. Department of Energy (DOE) Biological and Environmental Research Program ORNL is managed by UT-Battelle, LLC, under contract DE-AC05-00OR22725 with the U.S. DOE. This manuscript has been authored by UT-Battelle, LLC, under contract no. DE-AC05-00OR22725 with the US Department of Energy (DOE). The US government retains and the publisher, by accepting the article for publication, acknowledges that the US government retains a nonexclusive, paid-up, irrevocable, worldwide license to publish or reproduce the published form of this manuscript or allow others to do so, for US government purposes. DOE will provide public access to these results of federally sponsored research in accordance with the DOE Public Access Plan (http://energy.gov/downloads/doe-publicaccess-plan).

Author contribution

L.H. carried out model simulation, analyzed the model output, drafted the manuscript, and finalized reviewing and editing with contributions from other authors. J.R., M.M., C.L., and D.L. contributed to the experimental design and editing of the final version of the manuscript. X.X. developed the early version of the model, acquired funding, and contributed to model simulation design, result interpretation, and editing the manuscript.

Data availability statement

The sources of observational data for model validation have been clearly cited in the main text. The CLM-Microbe used in this study is available at the GitHub repository: https://github.com/email-clm/clm-microbe, and the model version used in this study has been archived (Xiaofeng Xu et al., 2022). The model outputs have been archived at the Dryad: https://doi.org/10.5061/dryad.612jm6471. Any other request can be directed to the corresponding author.

https://doi.org/10.5194/bg-2023-15
Preprint. Discussion started: 1 March 2023

Declaration of competing interest

The authors declare no competing interests.

Reference

Allison, S. D., Wallenstein, M. D., & Bradford, M. A. (2010). Soil-carbon response to warming dependent on microbial physiology. *Nature Geoscience*, *3*(5), 336-340. https://www.nature.com/articles/ngeo846

Bailey, V. L., Smith, J. L., & Bolton, H. (2002). Fungal-to-bacterial ratios in soils investigated for enhanced C sequestration. *Soil Biology and Biochemistry*, *34*(7), 997-1007. https://www.sciencedirect.com/science/article/pii/S0038071702000330

Boer, W. d., Folman, L. B., Summerbell, R. C., & Boddy, L. (2005). Living in a fungal world: impact of fungi on soil bacterial niche development. *FEMS Microbiology Reviews*, *29*(4), 795-811. https://academic.oup.com/femsre/article/29/4/795/493265

Bonan, G. B., Lombardozzi, D. L., Wieder, W. R., Oleson, K. W., Lawrence, D. M., Hoffman, F. M., & Collier, N. (2019). Model structure and climate data uncertainty in historical simulations of the terrestrial carbon cycle (1850–2014). *Global biogeochemical cycles*, *33*(10), 1310-1326. https://agupubs.onlinelibrary.wiley.com/doi/full/10.1029/2019GB006175

Bond-Lamberty, B., Bailey, V. L., Chen, M., Gough, C. M., & Vargas, R. (2018). Globally rising soil heterotrophic respiration over recent decades. *Nature*, *560*(7716), 80-83. https://www.nature.com/articles/s41586-018-0358-x

Bond-Lamberty, B., & Thomson, A. (2010). Temperature-associated increases in the global soil respiration record. *Nature*, *464*(7288), 579-582. https://www.nature.com/articles/nature08930/

Cheng, S., Huang, J., Ji, F., & Lin, L. (2017). Uncertainties of soil moisture in historical simulations and future projections. *Journal of Geophysical Research: Atmospheres*, *122*(4), 2239-2253. https://agupubs.onlinelibrary.wiley.com/doi/full/10.1002/2016JD025871

Cramer, W., Kicklighter, D. W., Bondeau, A., Iii, B. M., Churkina, G., Nemry, B., et al. (1999). Comparing global models of terrestrial net primary productivity (NPP): overview and key results. *Global change biology*, *5*(S1), 1-15. https://onlinelibrary.wiley.com/doi/abs/10.1046/j.1365-2486.1999.00009.x

https://onlinelibrary.wiley.com/doi/full/10.1046/j.1365-2486.1999.00009.x

Delire, C., Séférian, R., Decharme, B., Alkama, R., Calvet, J.-C., Carrer, D., et al. (2020). The global land carbon cycle simulated with ISBA-CTRIP: Improvements over the last decade. *Journal of Advances in Modeling Earth Systems*, *12*(9), e2019MS001886. https://agupubs.onlinelibrary.wiley.com/doi/full/10.1029/2019MS001886

Demoling, F., Nilsson, L. O., & Bååth, E. (2008). Bacterial and fungal response to nitrogen fertilization in three coniferous forest soils. *Soil Biology and Biochemistry*, *40*(2), 370-379. https://www.sciencedirect.com/science/article/pii/S0038071707003549

Dirmeyer, P. A., Gao, X., Zhao, M., Guo, Z., Oki, T., & Hanasaki, N. (2006). GSWP-2: Multimodel Analysis and Implications for Our Perception of the Land Surface. *Bulletin of the American Meteorological Society*, *87*(10), 1381-1398. https://journals.ametsoc.org/view/journals/bams/87/10/bams-87-10-1381.xml

Dusenge, M. E., Duarte, A. G., & Way, D. A. (2019). Plant carbon metabolism and climate change: elevated CO_2 and temperature impacts on photosynthesis, photorespiration and respiration. *New Phytologist*, *221*(1), 32-49. https://nph.onlinelibrary.wiley.com/doi/full/10.1111/nph.15283

Eglin, T., Ciais, P., Piao, S. L., Barré, P., Bellassen, V., Cadule, P., et al. (2010). Historical and future perspectives of global soil carbon response to climate and land-use changes. *Tellus B: Chemical and Physical Meteorology*, *62*(5), 700-718. https://www.tandfonline.com/doi/abs/10.1111/j.1600-0889.2010.00499.x

https://www.tandfonline.com/doi/pdf/10.1111/j.1600-0889.2010.00499.x

Ettema, C. H., & Wardle, D. A. (2002). Spatial soil ecology. *Trends in ecology & evolution*, *17*(4), 177-183. https://www.sciencedirect.com/science/article/pii/S0169534702024965

https://www.sciencedirect.com/science/article/pii/S0169534702024965/pdfft?md5=f393dd551648c40a3c186ad5535c025b&pid=1-s2.0-S0169534702024965-main.pdf&isDTMRedir=Y

FAO. (2018). *Global Soil Organic Carbon Map (GSOCmap) : Technical Report*. Rome, Italy: FAO.

Flato, G. M. (2011). Earth system models: an overview. *Wiley Interdisciplinary Reviews: Climate Change*, *2*(6), 783-800. https://onlinelibrary.wiley.com/doi/full/10.1002/wcc.148

Gabet, E. J., Reichman, O. J., & Seabloom, E. W. (2003). The effects of bioturbation on soil processes and sediment transport. *Annual Review of Earth and Planetary Sciences*, *31*(1), 249-273. https://www.annualreviews.org/doi/abs/10.1146/annurev.earth.31.100901.141314

Galloway, J. N., Townsend, A. R., Erisman, J. W., Bekunda, M., Cai, Z., Freney, J. R., et al. (2008). Transformation of the nitrogen cycle: recent trends, questions, and potential solutions. *Science*, *320*(5878), 889-892. https://www.science.org/doi/full/10.1126/science.1136674

Gomez-Casanovas, N., Matamala, R., Cook, D. R., & Gonzalez-Meler, M. A. (2012). Net ecosystem exchange modifies the relationship between the autotrophic and heterotrophic components of soil respiration with abiotic factors in prairie grasslands. *Global change biology*, *18*(8), 2532-2545. https://onlinelibrary.wiley.com/doi/full/10.1111/j.1365-2486.2012.02721.x

Guo, Z., Wang, Y., Wan, Z., Zuo, Y., He, L., Li, D., et al. (2020). Soil dissolved organic carbon in terrestrial ecosystems: Global budget, spatial distribution and controls. *Global Ecology and Biogeography*. https://onlinelibrary.wiley.com/doi/full/10.1111/geb.13186

Hashimoto, S., Carvalhais, N., Ito, A., Migliavacca, M., Nishina, K., & Reichstein, M. (2015). Global spatiotemporal distribution of soil respiration modeled using a global database. *Biogeosciences*, *12*(13), 4121-4132. https://bg.copernicus.org/articles/12/4121/2015/

He, L., Lai, C.-T., Mayes, M. A., Murayama, S., & Xu, X. (2021). Microbial seasonality promotes soil respiratory carbon emission in natural ecosystems: a modeling study. *Global change biology*, *27*(13), 3035-3051.

He, L., Lipson, D. A., Rodrigues, J. L. M., Mayes, M., Björk, R. G., Glaser, B., et al. (2021). Dynamics of Fungal and Bacterial Biomass Carbon in Natural Ecosystems: Site-level Applications of the CLM-Microbe Model. *Journal of Advances in Modeling Earth Systems*, *13*(2), e2020MS002283. https://agupubs.onlinelibrary.wiley.com/doi/abs/10.1029/2020MS002283

He, L., Rodrigues, J. L. M., Soudzilovskaia, N. A., Barceló, M., Olsson, P. a. A., Song, C., et al. (2020). Global biogeography of fungal and bacterial biomass carbon in topsoil. *Soil Biology and Biochemistry*, 108024. https://www.sciencedirect.com/science/article/pii/S0038071720303205

He, L., & Xu, X. (2021). Mapping soil microbial residence time at the global scale. *Global change biology*, *27*(24), 6484-6497. https://onlinelibrary.wiley.com/doi/abs/10.1111/gcb.15864

https://doi.org/10.5194/bg-2023-15
Preprint. Discussion started: 1 March 2023

Hršelová, H., Chvátalová, I., Vosátka, M., Klír, J., & Gryndler, M. (1999). Correlation of abundance of arbuscular mycorrhizal fungi, bacteria and saprophytic microfungi with soil carbon, nitrogen and phsophorus. *Folia microbiologica*, *44*(6), 683-687. https://link.springer.com/article/10.1007/BF02825662

https://link.springer.com/content/pdf/10.1007/BF02825662.pdf

Huang, N., Wang, L., Song, X.-P., Black, T. A., Jassal, R. S., Myneni, R. B., et al. (2020). Spatial and temporal variations in global soil respiration and their relationships with climate and land cover. *Science advances*, *6*(41), eabb8508. https://www.science.org/doi/full/10.1126/sciadv.abb8508

IPCC. (2001). Climate change 2001 : the scientific basis. *Contribution of Working Group I to the Third Assessment Report of the Intergovernmental Panel on Climate Change*, *2001*. https://ci.nii.ac.jp/naid/10027437043/

IPCC. (2013). *Summary for policymakers*. Retrieved from Cambridge, United Kingdom and New York, NY, USA:

Kassambara, A., & Kassambara, M. A. (2019). Package 'ggcorrplot'. *R package version 0.1*, *3*(3).

Kim, D., Lee, M.-I., & Seo, E. (2019). Improvement of soil respiration parameterization in a dynamic global vegetation model and its impact on the simulation of terrestrial carbon fluxes. *Journal of Climate*, *32*(1), 127-143. https://journals.ametsoc.org/view/journals/clim/32/1/jcli-d-18-0018.1.xml

Koven, C. D., Riley, W. J., Subin, Z. M., Tang, J. Y., Torn, M. S., Collins, W. D., et al. (2013). The effect of vertically resolved soil biogeochemistry and alternate soil C and N models on C dynamics of CLM4. *Biogeosciences*, *10*(11), 7109. https://bg.copernicus.org/articles/10/7109/2013/

Kuzyakov, Y., & Blagodatskaya, E. (2015). Microbial hotspots and hot moments in soil: Concept & review. *Soil Biology and Biochemistry*, *83*, 184-199. https://www.sciencedirect.com/science/article/pii/S0038071715000449

https://www.sciencedirect.com/science/article/pii/S0038071715000449#bib104

Lal, R. (2004). Soil carbon sequestration to mitigate climate change. *Geoderma*, *123*(1-2), 1-22. https://www.sciencedirect.com/science/article/pii/S0016706104000266

Lal, R. (2008). Promise and limitations of soils to minimize climate change. *Journal of Soil and Water Conservation*, *63*(4), 113A-118A. https://www.jswconline.org/content/jswc/63/4/113A.full.pdf

Lu, H., Li, S., Ma, M., Bastrikov, V., Chen, X., Ciais, P., et al. (2021). Comparing machine learning-derived global estimates of soil respiration and its components with those from terrestrial ecosystem models. *Environmental Research Letters*, *16*(5), 054048. https://iopscience.iop.org/article/10.1088/1748-9326/abf526/meta

https://iopscience.iop.org/article/10.1088/1748-9326/abf526/pdf

Manzoni, S., Schimel, J. P., & Porporato, A. (2012). Responses of soil microbial communities to water stress: results from a meta-analysis. *Ecology*, *93*(4), 930-938. https://esajournals.onlinelibrary.wiley.com/doi/full/10.1890/11-0026.1

Mathieu, P.-P., & O'Neill, A. (2008). Data assimilation: From photon counts to Earth System forecasts. *Remote Sensing of Environment*, *112*(4), 1258-1267. https://www.sciencedirect.com/science/article/pii/S0034425707003240

https://www.sciencedirect.com/science/article/pii/S0034425707003240/pdfft?md5=cb5db33089a276663a7611ce0e63db89&pid=1-s2.0-S0034425707003240-main.pdf&isDTMRedir=Y

Matson, P., Lohse, K. A., & Hall, S. J. (2002). The globalization of nitrogen deposition: consequences for terrestrial ecosystems. *Ambio*, 113-119. https://www.jstor.org/stable/4315223

https://www.jstor.org/stable/pdf/4315223.pdf

Meeran, K., Ingrisch, J., Reinthaler, D., Canarini, A., Müller, L., Pötsch, E. M., et al. (2021). Warming and elevated CO_2 intensify drought and recovery responses of grassland carbon allocation to soil respiration. *Global change biology*, *27*(14), 3230-3243. https://doi.org/10.1111/gcb.15628. https://doi.org/10.1111/gcb.15628

Nemani, R. R., Keeling, C. D., Hashimoto, H., Jolly, W. M., Piper, S. C., Tucker, C. J., et al. (2003). Climate-driven increases in global terrestrial net primary production from 1982 to 1999. *Science*, *300*(5625), 1560-1563. https://www.science.org/doi/full/10.1126/science.1082750

Noh, N. J., Kuribayashi, M., Saitoh, T. M., & Muraoka, H. (2017). Different responses of soil, heterotrophic and autotrophic respirations to a 4-year soil warming experiment in a cool-temperate deciduous broadleaved forest in central Japan. *Agricultural and Forest Meteorology*, *247*, 560-570. https://www.sciencedirect.com/science/article/pii/S0168192317302976

Pascual, J. A., García, C., Hernandez, T., & Ayuso, M. (1997). Changes in the microbial activity of an arid soil amended with urban organic wastes. *Biology and Fertility of Soils*, *24*(4), 429-434. https://doi.org/10.1007/s003740050268

Pendall, E., Bridgham, S., Hanson, P. J., Hungate, B., Kicklighter, D. W., Johnson, D. W., et al. (2004). Below-ground process responses to elevated CO2 and temperature: a discussion of observations, measurement methods, and models. *New Phytologist*, *162*(2), 311-322. https://onlinelibrary.wiley.com/doi/abs/10.1111/j.1469-8137.2004.01053.x https://nph.onlinelibrary.wiley.com/doi/full/10.1111/j.1469-8137.2004.01053.x

Pietikäinen, J., Pettersson, M., & Bååth, E. (2005). Comparison of temperature effects on soil respiration and bacterial and fungal growth rates. *FEMS Microbiology Ecology*, *52*(1), 49-58.

Piñeiro, J., Ochoa-Hueso, R., Delgado-Baquerizo, M., Dobrick, S., Reich, P. B., Pendall, E., & Power, S. A. (2017). Effects of elevated CO2 on fine root biomass are reduced by aridity but enhanced by soil nitrogen: A global assessment. *Scientific reports*, *7*(1), 1-9. https://www.nature.com/articles/s41598-017-15728-4

Prescott, C. E., Grayston, S. J., Helmisaari, H.-S., Kaštovská, E., Körner, C., Lambers, H., et al. (2020). Surplus carbon drives allocation and plant–soil interactions. *Trends in ecology & evolution*, *35*(12), 1110-1118. https://www.sciencedirect.com/science/article/pii/S0169534720302226

Preusser, S., Poll, C., Marhan, S., Angst, G., Mueller, C. W., Bachmann, J., & Kandeler, E. (2019). Fungi and bacteria respond differently to changing environmental conditions within a soil profile. *Soil Biology and Biochemistry*, *137*, 107543. https://www.sciencedirect.com/science/article/pii/S003807171930207X

Qiu, S., McComb, A. J., Bell, R. W., & Davis, J. A. (2005). Response of soil microbial activity to temperature, moisture, and litter leaching on a wetland transect during seasonal refilling. *Wetlands Ecology and Management*, *13*(1), 43-54.

R Core Team. (2013). R: A language and environment for statistical computing. Vienna, Austria: R Foundation for Statistical Computing. *Available*.

Rousk, J., & Bååth, E. (2011). Growth of saprotrophic fungi and bacteria in soil. *FEMS Microbiology Ecology*, *78*(1), 17-30.

Sampaio, G., Nobre, C., Costa, M. H., Satyamurty, P., Soares-Filho, B. S., & Cardoso, M. (2007). Regional climate change over eastern Amazonia caused by pasture and soybean cropland expansion. *Geophysical Research Letters*, *34*(17). https://agupubs.onlinelibrary.wiley.com/doi/full/10.1029/2007GL030612

Schimel, D. S. (1995). Terrestrial ecosystems and the carbon cycle. *Global change biology*, *1*(1), 77-91. https://onlinelibrary.wiley.com/doi/abs/10.1111/j.1365-2486.1995.tb00008.x

Schimel, J. P. (2018). Life in dry soils: effects of drought on soil microbial communities and processes. *Annual review of ecology, evolution, and systematics*, *49*, 409-432. https://www.annualreviews.org/doi/full/10.1146/annurev-ecolsys-110617-062614

Sinsabaugh, R. L., Turner, B. L., Talbot, J. M., Waring, B. G., Powers, J. S., Kuske, C. R., et al. (2016). Stoichiometry of microbial carbon use efficiency in soils. *Ecological Monographs*, *86*(2), 172-189. https://esajournals.onlinelibrary.wiley.com/doi/full/10.1890/15-2110.1

Soong, J. L., Castanha, C., Pries, C. E. H., Ofiti, N., Porras, R. C., Riley, W. J., et al. (2021). Five years of whole-soil warming led to loss of subsoil carbon stocks and increased CO_2 efflux. *Science advances, 7*(21), eabd1343. https://www.science.org/doi/abs/10.1126/sciadv.abd1343

Stevenson, B. A., Sarmah, A. K., Smernik, R., Hunter, D. W. F., & Fraser, S. (2016). Soil carbon characterization and nutrient ratios across land uses on two contrasting soils: Their relationships to microbial biomass and function. *Soil Biology and Biochemistry, 97*, 50-62. https://www.sciencedirect.com/science/article/pii/S0038071716000560

Thornton, P. E., & Rosenbloom, N. A. (2005). Ecosystem model spin-up: Estimating steady state conditions in a coupled terrestrial carbon and nitrogen cycle model. *Ecological Modelling, 189*(1-2), 25-48. https://www.sciencedirect.com/science/article/pii/S0304380005001948

Todd-Brown, K. E. O., Randerson, J. T., Post, W. M., Hoffman, F. M., Tarnocai, C., Schuur, E. A. G., & Allison, S. D. (2013). Causes of variation in soil carbon simulations from CMIP5 Earth system models and comparison with observations. *Biogeosciences, 10*(3), 1717-1736. https://bg.copernicus.org/articles/10/1717/2013/

Van Damme, M., Clarisse, L., Franco, B., Sutton, M. A., Erisman, J. W., Wichink Kruit, R., et al. (2021). Global, regional and national trends of atmospheric ammonia derived from a decadal (2008–2018) satellite record. *Environmental Research Letters, 16*(5), 055017. http://dx.doi.org/10.1088/1748-9326/abd5e0

Vance, E. D., & Chapin, I. F. S. (2001). Substrate limitations to microbial activity in taiga forest floors. *Soil Biology and Biochemistry, 33*(2), 173-188. https://www.sciencedirect.com/science/article/pii/S0038071700001279

Viovy, N. (2018). *CRUNCEP Version 7 - Atmospheric Forcing Data for the Community Land Model*. Retrieved from: https://doi.org/10.5065/PZ8F-F017

Wang, G., Jagadamma, S., Mayes, M. A., Schadt, C. W., Steinweg, J. M., Gu, L., & Post, W. M. (2015). Microbial dormancy improves development and experimental validation of ecosystem model. *The ISME Journal, 9*(1), 226-237. https://www.nature.com/articles/ismej2014120

Wang, K., Peng, C., Zhu, Q., Zhou, X., Wang, M., Zhang, K., & Wang, G. (2017). Modeling global soil carbon and soil microbial carbon by integrating microbial processes into the ecosystem process model TRIPLEX-GHG. *Journal of Advances in Modeling Earth Systems, 9*(6), 2368-2384. https://agupubs.onlinelibrary.wiley.com/doi/abs/10.1002/2017MS000920

Wang, Y., Yuan, F., Arndt, K. A., Liu, J., He, L., Zuo, Y., et al. (2022). Upscaling methane flux from plot-level to eddy covariance tower domains in five Alaskan tundra ecosystems. *Frontiers in Environmental Science, 10*, 10.3389/fenvs.2022.939238.

Wang, Y., Yuan, F., Yuan, F., Gu, B., Hahn, M. S., Torn, M. S., et al. (2019). Mechanistic modeling of microtopographic impacts on CO_2 and CH_4 Fluxes in an Alaskan tundra ecosystem using the CLM-Microbe model. *Journal of Advances in Modeling Earth Systems, 11*, 17. https://agupubs.onlinelibrary.wiley.com/doi/full/10.1029/2019MS001771

Wardle, D. A., & Parkinson, D. (1990). Interactions between microclimatic variables and the soil microbial biomass. *Biology and Fertility of Soils, 9*(3), 273-280. https://doi.org/10.1007/BF00336239

Warner, D. L., Bond-Lamberty, B. P., Jian, J., Stell, E., & Vargas, R. (2019). Global Gridded 1-km Annual Soil Respiration and Uncertainty Derived from SRDB V3. In: ORNL Distributed Active Archive Center.

Wieder, W. (2014). Regridded Harmonized World Soil Database v1.2. In: ORNL Distributed Active Archive Center.

Wieder, W. R., Bonan, G. B., & Allison, S. D. (2013). Global soil carbon projections are improved by modelling microbial processes. *Nature Climate Change, 3*(10), 909-912. https://www.nature.com/articles/nclimate1951

Wieder, W. R., Grandy, A. S., Kallenbach, C. M., Taylor, P. G., & Bonan, G. B. (2015). Representing life in the Earth system with soil microbial functional traits in the MIMICS model. *Geoscientific Model Development, 8*, 1789-1808. http://adsabs.harvard.edu/abs/2015GMD.....8.1789W

Wiltshire, A. J., Burke, E. J., Chadburn, S. E., Jones, C. D., Cox, P. M., Davies-Barnard, T., et al. (2021). JULES-CN: a coupled terrestrial carbon–nitrogen scheme (JULES vn5. 1). *Geoscientific Model Development, 14*(4), 2161-2186.

Xu, X., Elias, D. A., Graham, D. E., Phelps, T. J., Carroll, S. L., Wullschleger, S. D., & Thornton, P. E. (2015). A microbial functional group-based module for simulating methane production and consumption: Application to an incubated permafrost soil. *Journal of Geophysical Research: Biogeosciences, 120*(7), 1315-1333. https://agupubs.onlinelibrary.wiley.com/doi/abs/10.1002/2015JG002935

Xu, X., He, L., & Wang, Y. (2022). CLM-Microbe v1.0. [software] *Zenodo, https://doi.org/10.5281/zenodo.7439312*.

Xu, X., Schimel, J. P., Thornton, P. E., Song, X., Yuan, F., & Goswami, S. (2014). Substrate and environmental controls on microbial assimilation of soil organic carbon: a framework for Earth system models. *Ecology Letters, 17*(5), 547-555. https://doi.org/10.1111/ele.12254

Xu, X., Thornton, P. E., & Post, W. M. (2013). A global analysis of soil microbial biomass carbon, nitrogen and phosphorus in terrestrial ecosystems. *Global Ecology and Biogeography, 22*(6), 737-749.

Xu, X., Wang, N., Lipson, D. L., Sinsabaugh, R. L., Schimel, J. P., He, L., et al. (2020). Microbial macroecology: in search of mechanisms governing microbial biogeographic patterns. *Global Ecology and Biogeography, 29*, 1870-1886.

Xu, X. F., Tian, H. Q., Zhang, C., Liu, M. L., Ren, W., Chen, G. S., et al. (2010). Attribution of spatial and temporal variations in terrestrial methane flux over North America. *Biogeosciences, 7*(11), 3637-3655.

Yue, X., Unger, N., & Zheng, Y. (2015). Distinguishing the drivers of trends in land carbon fluxes and plant volatile emissions over the past 3 decades. *Atmospheric Chemistry and Physics, 15*(20), 11931-11948. https://acp.copernicus.org/articles/15/11931/2015/

Zhang, Q., Lei, H.-M., & Yang, D.-W. (2013). Seasonal variations in soil respiration, heterotrophic respiration and autotrophic respiration of a wheat and maize rotation cropland in the North China Plain. *Agricultural and Forest Meteorology, 180*, 34-43. https://www.sciencedirect.com/science/article/pii/S0168192313001056

Zhao, M., Heinsch, F. A., Nemani, R. R., & Running, S. W. (2005). Improvements of the MODIS terrestrial gross and net primary production global data set. *Remote Sensing of Environment, 95*(2), 164-176. https://www.sciencedirect.com/science/article/pii/S0034425705000106

Zhao, Z., Peng, C., Yang, Q., Meng, F.-R., Song, X., Chen, S., et al. (2017). Model prediction of biome-specific global soil respiration from 1960 to 2012. *Earth's Future, 5*(7), 715-729. https://onlinelibrary.wiley.com/doi/abs/10.1002/2016EF000480

Zheng, Y., Shen, R., Wang, Y., Li, X., Liu, S., Liang, S., et al. (2020). Improved estimate of global gross primary production for reproducing its long-term variation, 1982–2017. *Earth System Science Data, 12*(4), 2725-2746.

Zhou, L., Zhou, X., Shao, J., Nie, Y., He, Y., Jiang, L., et al. (2016). Interactive effects of global change factors on soil respiration and its components: a meta-analysis. *Global Change Biology, 22*(9), 3157-3169. https://onlinelibrary.wiley.com/doi/full/10.1111/gcb.13253

Zhou, X., Wan, S., & Luo, Y. (2007). Source components and interannual variability of soil CO_2 efflux under experimental warming and clipping in a grassland ecosystem. *Global Change Biology, 13*(4), 761-775. https://onlinelibrary.wiley.com/doi/full/10.1111/j.1365-2486.2007.01333.x

https://doi.org/10.5194/bg-2023-15
Preprint. Discussion started: 1 March 2023

Zhu, X., Zhang, L., Zuo, Y., Liu, J., Yu, J., Yuan, F., et al. (2021). Wetland reclamation homogenizes microbial properties along soil profiles. *Geoderma*, *395*, 115075. https://www.sciencedirect.com/science/article/pii/S001670612100149X

https://doi.org/10.5194/bg-2023-15
Preprint. Discussion started: 1 March 2023

Table 1. Annual flux of GPP, NPP, HR, and SR and carbon stocks of FBC in the top 30 cm, BBC in the top 30 cm, MBC (0-1 m), DOC in the top 30 cm, SOC in the top 30 cm, and SOC in the top 1 m by observed datasets and by simulations of the CLM-Microbe model and CLM4.5 at the global scale

		Global estimation		
Variables	Unit	Observed	CLM-Microbe	CLM4.5
GPP	PgC yr^{-1}	111.94	129.53	120.13
NPP		55.76	56.49	51.26
SR		86.34	99.80	89.79
HR		49.01	49.84	46.87
FBC (0-30 cm)	PgC	13.57	13.12	--
BBC (0-30 cm)		3.29	4.17	--
MBC (0-1 m)		23.70	40.18	--
DOC (0-30 cm)		7.16	8.94	--
DOC (0-1 m)		12.90	22.57	--
SOC (0-30 cm)		661.71	605.27	513.40
SOC (0-1 m)		1231.99	1630.90	967.87

GPP: gross primary productivity; NPP: net primary productivity; HR: heterotrophic respiration; SR: soil respiration; DOC: dissolved organic carbon; SOC: soil organic carbon; FBC: fungal biomass carbon; BBC: bacterial biomass carbon; MBC: microbial biomass carbon. -- denoted not available. The SOC (0-1 m) data were from the Harmonized World Soil Database (HWSD, https://daac.ornl.gov/cgi-bin/dsviewer.pl?ds_id=1247); the SOC (0-30 cm) data were from the Global Soil Organic Carbon Map (GSOCmap) version 1.5; GPP and NPP data were from MODIS gridded datasets (http://files.ntsg.umt.edu/data/NTSG_Products/); the SR and HR data were from Global Gridded 1-km Annual Soil Respiration Database (SRDB) version 3 (https://daac.ornl.gov/CMS/guides/CMS_Global_Soil_Respiration.html); the FBC and BBC in the top 30 cm were from He et al. (2020); MBC (0-1 m) was compared with Xiaofeng Xu et al. (2013); the DOC (0-30 cm and 0-1 m) was derived from Guo et al. (2020). Output of the CLM-Microbe model during 2000-2009 (decadal average) were used to compare with observational data.

https://doi.org/10.5194/bg-2023-15
Preprint. Discussion started: 1 March 2023

Table 2. Carbon stock of vegetation, litter, and soil pools and absolute and relative changes from 1901-1910 to 2007-2016

	Total Carbon stock (PgC)		Change from 1901-1910 to 2007-2016	
Pool	1901-1910	2007-2016	Absolute change (PgC)	Relative change (%)
SOC	4527 (0.4)	4564 (1.8)	37.0*	0.8
Litter	63 (0.2)	68 (0.4)	5.1*	8.0
Vegetation	193 (1.1)	230 (2.9)	37.1*	19.2

Numbers in parentheses represent standard deviation. * indicates significant absolute change from 1901-1910 to 2007-2016 at $\alpha = 0.05$.

https://doi.org/10.5194/bg-2023-15
Preprint. Discussion started: 1 March 2023

Table 3. Decadal averages of GPP, NPP, HR, and SR and carbon stocks of FBC in the top 30 cm, FBC in the top 1 m, BBC in the top 30 cm, BBC in the top 1 m, DOC in the top 1 m, and SOC in the top 1 m and their absolute and relative changes by simulations of the CLM-Microbe model at the continental scale

			Continent						
	Variables	Unit	Asia	North America	Europe	Africa	South America	Australia/ Oceania	Globe
1901-1910	GPP	PgC yr^{-1}	28.7 (0.50)	16.6 (0.48)	9.2 (0.26)	20.8 (0.25)	31.0 (0.48)	3.3 (0.28)	109.6 (1.14)
	NPP		12.2 (0.27)	7.3 (0.16)	4.3 (0.10)	9.4 (0.22)	12.3 (0.53)	1.5 (0.15)	46.9 (0.78)
	HR		11.1 (0.19)	6.7 (0.25)	4.0 (0.16)	8.0 (0.16)	11.1 (0.25)	1.3 (0.12)	42.2 (0.57)
	SR		22.1 (0.46)	13.7 (0.40)	7.7 (0.20)	15.3 (0.22)	21.7 (0.39)	2.7 (0.22)	83.2 (1.31)
	FBC (0-30 cm)	PgC	4.5 (0.01)	3.5 (0.02)	1.3 (0.01)	1.5 (0.01)	1.9 (0.01)	0.4 (0.00)	13.0 (0.04)
	FBC (0-1 m)		10.3 (0.02)	7.8 (0.04)	2.7 (0.04)	3.6 (0.00)	5.5 (0.01)	0.9 (0.00)	30.8 (0.08)
	BBC (0-30 cm)		1.4 (0.00)	1.0 (0.01)	0.4 (0.00)	0.4 (0.00)	0.7 (0.01)	0.1 (0.00)	4.1 (0.02)
	BBC (0-1 m)		3.6 (0.01)	2.3 (0.01)	0.9 (0.01)	1.2 (0.00)	2.5 (0.01)	0.2 (0.00)	10.7 (0.03)
	DOC (0-1 m)		7.5 (0.02)	6.5 (0.02)	2.6 (0.03)	1.9 (0.00)	2.7 (0.00)	0.6 (0.00)	21.9 (0.07)
	SOC (0-1 m)		563.8 (0.12)	415.9 (0.06)	206.4 (0.03)	170.8 (0.11)	311.3 (0.15)	29.6 (0.01)	1697.9 (0.45)
	VegC		49.9 (0.28)	23.3 (0.33)	12.5 (0.13)	34.6 (0.26)	69.8 (0.47)	3.2 (0.20)	193.3 (1.12)
	LitC (0-1 m)		8.5 (0.03)	3.1 (0.04)	1.1 (0.04)	5.6 (0.05)	13.5 (0.09)	0.7 (0.03)	32.5 (0.18)
2007-2016	GPP	PgC yr^{-1}	38.1 (0.31)	20.9 (0.39)	12.4 (0.22)	25.8 (0.40)	38.3 (0.54)	4.1 (0.23)	139.6 (0.77)
	NPP		16.3 (0.32)	9.2 (0.14)	5.8 (0.16)	11.6 (0.24)	15.3 (0.56)	1.8 (0.12)	60.1 (0.99)
	HR		14.7 (0.20)	8.3 (0.24)	5.4 (0.22)	9.8 (0.25)	13.8 (0.37)	1.7 (0.15)	53.6 (0.65)
	SR		30.1 (0.38)	17.2 (0.36)	10.4 (0.24)	19.4 (0.35)	27.5 (0.47)	3.4 (0.26)	108.0 (1.16)
	FBC (0-30 cm)	PgC	4.8 (0.03)	3.8 (0.02)	1.4 (0.01)	1.6 (0.01)	2.1 (0.01)	0.4 (0.01)	14.1 (0.07)
	FBC (0-1 m)		10.7 (0.05)	8.0 (0.03)	2.7 (0.02)	3.8 (0.01)	5.9 (0.02)	0.9 (0.01)	31.9 (0.14)
	BBC (0-30 cm)		1.6 (0.01)	1.1 (0.01)	0.5 (0.00)	0.5 (0.00)	0.8 (0.01)	0.1 (0.00)	4.5 (0.03)
	BBC (0-1 m)		3.7 (0.02)	2.4 (0.01)	1.0 (0.01)	1.3 (0.01)	2.6 (0.01)	0.2 (0.00)	11.3 (0.05)
	DOC (0-1 m)		8.3 (0.07)	7.2 (0.04)	3.0 (0.05)	2.1 (0.01)	3.1 (0.01)	0.6 (0.00)	24.3 (0.18)
	SOC (0-1 m)		572.8 (0.58)	421.4 (0.31)	212.3 (0.25)	176.5 (0.18)	318.9 (0.26)	30.3 (0.04)	1732.2 (1.62)
	VegC		58.7 (0.98)	29.0 (0.53)	16.5 (0.27)	39.0 (0.63)	83.2 (0.73)	3.9 (0.27)	230.4 (2.92)
	LitC (0-1 m)		9.6 (0.09)	3.5 (0.06)	1.3 (0.05)	6.3 (0.09)	15.0 (0.12)	0.8 (0.03)	36.5 (0.29)
Absolute change from 1901-1910 to 2007-2016	GPP	PgC yr^{-1}	9.39*	4.23*	3.20*	4.98*	7.32*	0.86*	30.0*
	NPP		4.11*	1.91*	1.55*	2.21*	2.99*	0.34*	13.1*
	HR		3.61*	1.62*	1.43*	1.79*	2.70*	0.31*	11.5*
	SR		8.02*	3.48*	2.76*	4.03*	5.83*	0.74*	24.9*
	FBC (0-30 cm)	PgC	0.35*	0.21*	0.10*	0.13*	0.22*	0.00	1.0*
	FBC (0-1 m)		0.37*	0.26*	-0.01	0.21*	0.38*	-0.04*	1.2*
	BBC (0-30 cm)		0.11*	0.07*	0.06*	0.05*	0.09*	0.00	0.4*
	BBC (0-1 m)		0.18*	0.11*	0.10*	0.09*	0.18*	-0.01*	0.7*
	DOC (0-1 m)		0.75*	0.67*	0.40*	0.21*	0.41*	-0.04*	2.4*
	SOC (0-1 m)		8.96*	5.46*	5.90*	5.67*	7.65*	0.69*	34.3*
	VegC		8.82*	5.71*	4.06*	4.46*	13.39*	0.68*	37.1*
	LitC (0-1 m)		1.06*	0.45*	0.26*	0.75*	1.42*	0.10*	4.0*
Relative change from 1901-1910 to 2007-2016	GPP	%	32.7	25.4	34.9	23.9	23.6	26.4	27.4
	NPP		33.6	26.3	36.0	23.6	24.4	23.0	27.9
	HR		32.5	24.2	36.0	22.3	24.4	23.1	27.2
	SR		36.2	25.5	36.0	26.2	26.9	27.9	29.9
	FBC (0-30 cm)		7.8	6.0	7.6	8.7	12.0	-0.9	7.8
	FBC (0-1 m)		3.6	3.3	-0.3	5.7	6.8	-4.2	3.8
	BBC (0-30 cm)		7.9	6.5	14.9	11.0	13.2	-1.9	9.3
	BBC (0-1 m)		5.0	4.9	11.5	7.4	7.3	-2.7	6.1
	DOC (0-1 m)		10.0	10.2	15.1	11.1	15.1	-7.2	10.9
	SOC (0-1 m)		1.6	1.3	2.9	3.3	2.5	2.3	2.0
	VegC		17.7	24.5	32.5	12.9	19.2	21.2	19.2
	LitC (0-1 m)		12.4	14.5	23.4	13.4	10.5	14.5	12.4

GPP: gross primary productivity; NPP: net primary productivity; HR: heterotrophic respiration; SR: soil respiration; DOC: dissolved organic carbon; SOC: soil organic carbon; FBC: fungal biomass carbon; BBC: bacterial biomass carbon. Numbers in parentheses represent standard deviation. * indicates significant absolute change from 1901-1910 to 2007-2016 at $\alpha = 0.05$.

https://doi.org/10.5194/bg-2023-15
Preprint. Discussion started: 1 March 2023

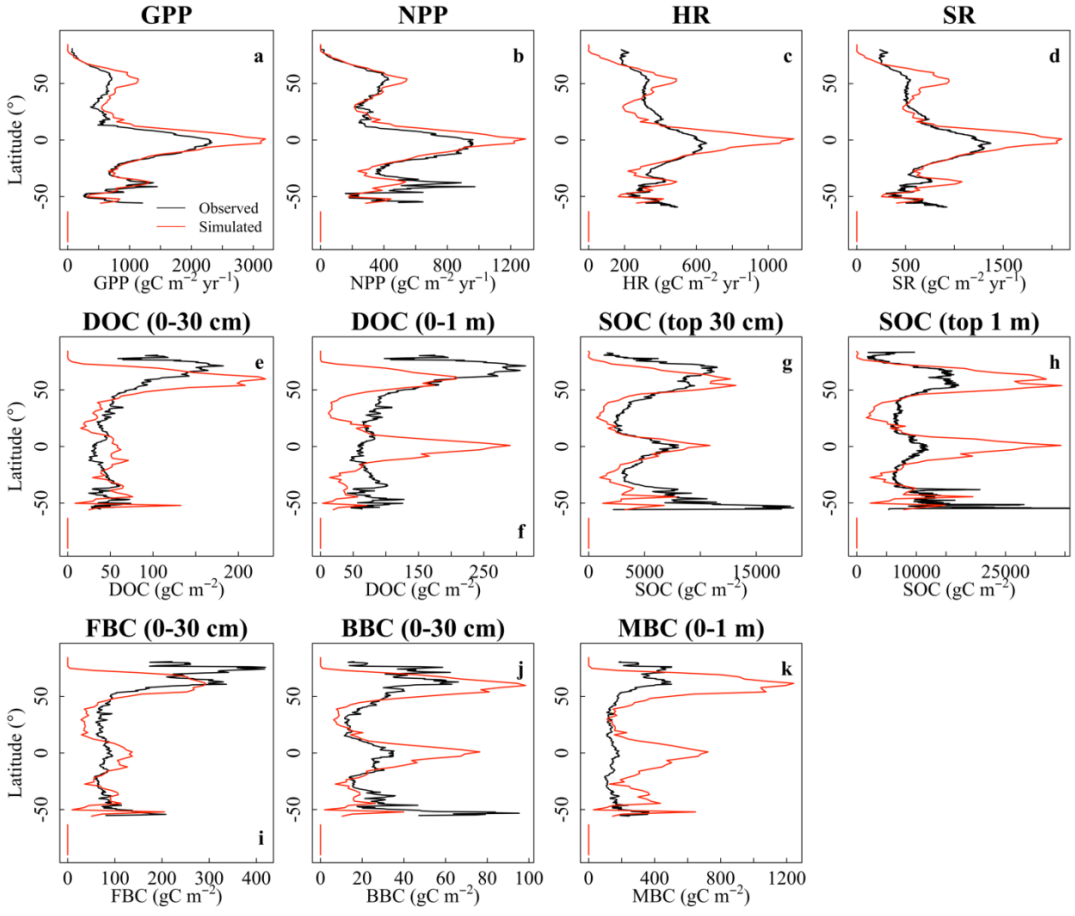

Fig. 1. Latitudinal comparison between observed (black line) and the CLM-Microbe-simulated (red line) (a) GPP, (b) NPP, (c) HR, (d) SR, (e) DOC in the top 30 cm, (f) DOC in the top 1 m, (g) SOC in the top 30 cm, (h) SOC in the top 1 m, (i) FBC in the top 30 cm, (j) BBC in the top 30 cm, and (k) MBC (0-1 m). GPP: gross primary productivity; NPP: net primary productivity; HR: heterotrophic respiration; SR: soil respiration; DOC: dissolved organic carbon; SOC: soil organic carbon; FBC: fungal biomass carbon; BBC: bacterial biomass carbon; MBC: microbial biomass carbon.

https://doi.org/10.5194/bg-2023-15
Preprint. Discussion started: 1 March 2023

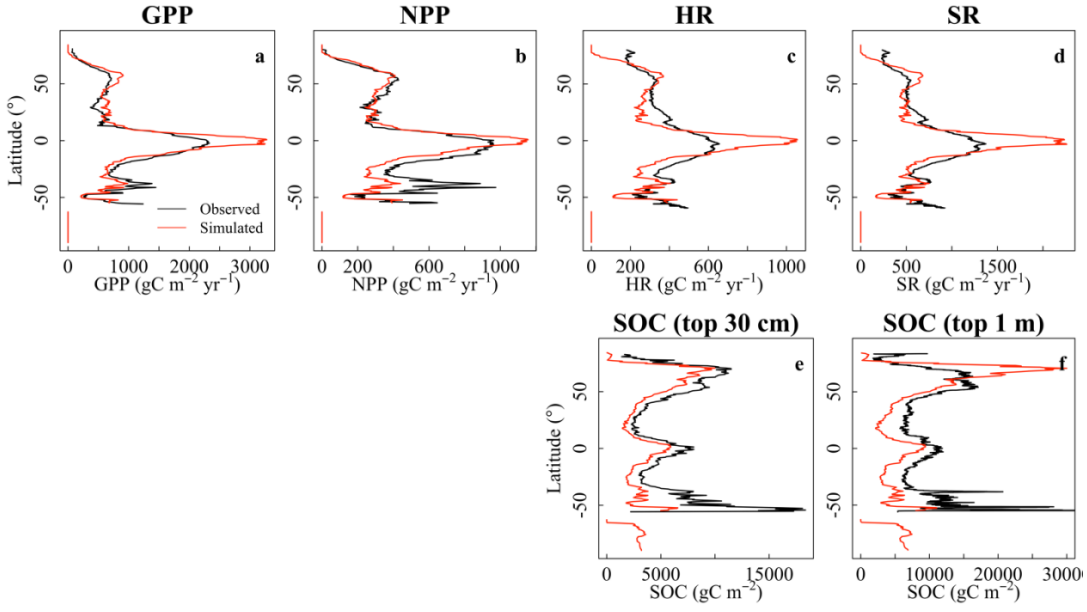

1080 **Fig. 2.** Latitudinal comparison between observed (black line) and the CLM4.5-simulated (red line) latitudinal gradients of (a) GPP, (b) NPP, (c) HR, (d) SR, (e) SOC in the top 30 cm, and (f) SOC in the top 1 m. GPP: gross primary productivity; NPP: net primary productivity; HR: heterotrophic respiration; SR: soil respiration; SOC: soil organic carbon.

https://doi.org/10.5194/bg-2023-15
Preprint. Discussion started: 1 March 2023

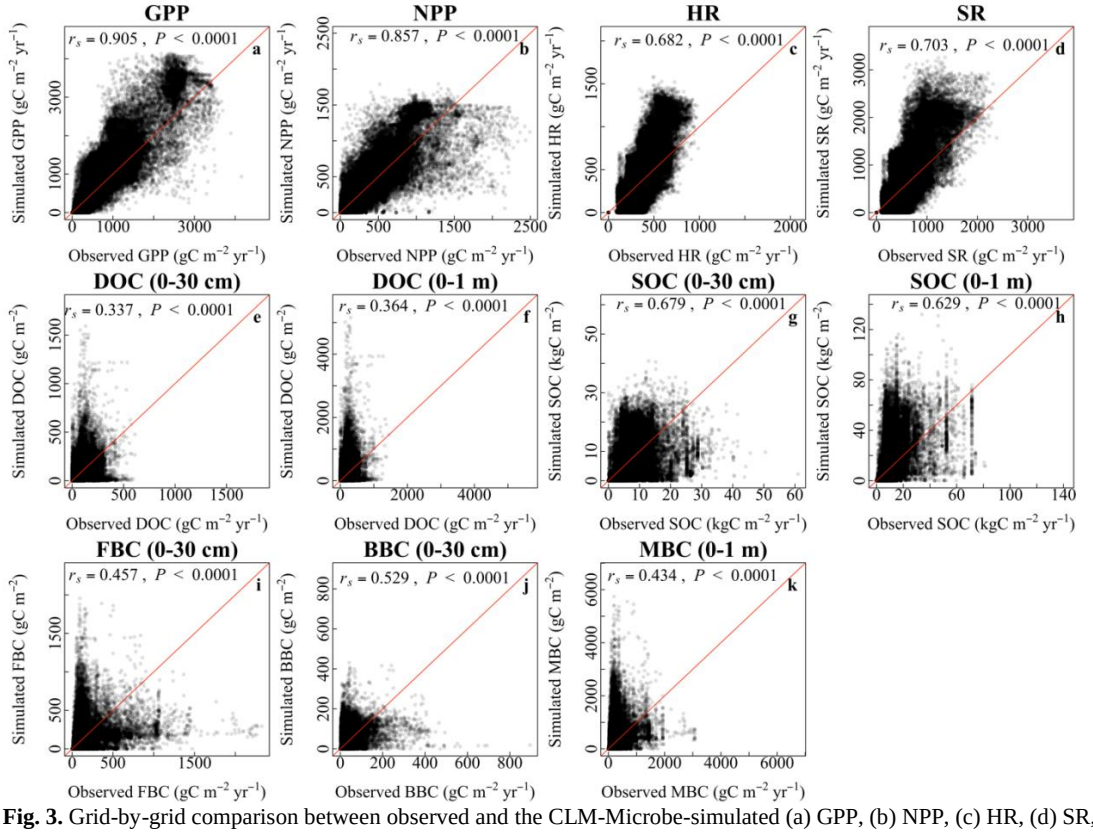

Fig. 3. Grid-by-grid comparison between observed and the CLM-Microbe-simulated (a) GPP, (b) NPP, (c) HR, (d) SR, (e) DOC in the top 30 cm, (f) DOC in the top 1 m, (g) SOC in the top 30 cm, (h) SOC in the top 1 m, (i) FBC in the top 30 cm, (j) BBC in the top 30 cm, and (k) MBC (0-1 m). Red lines are 1:1 line. GPP: gross primary productivity; NPP: net primary productivity; HR: heterotrophic respiration; SR: soil respiration; DOC: dissolved organic carbon; SOC: soil organic carbon; FBC: fungal biomass carbon; BBC: bacterial biomass carbon; MBC: microbial biomass carbon.

https://doi.org/10.5194/bg-2023-15
Preprint. Discussion started: 1 March 2023

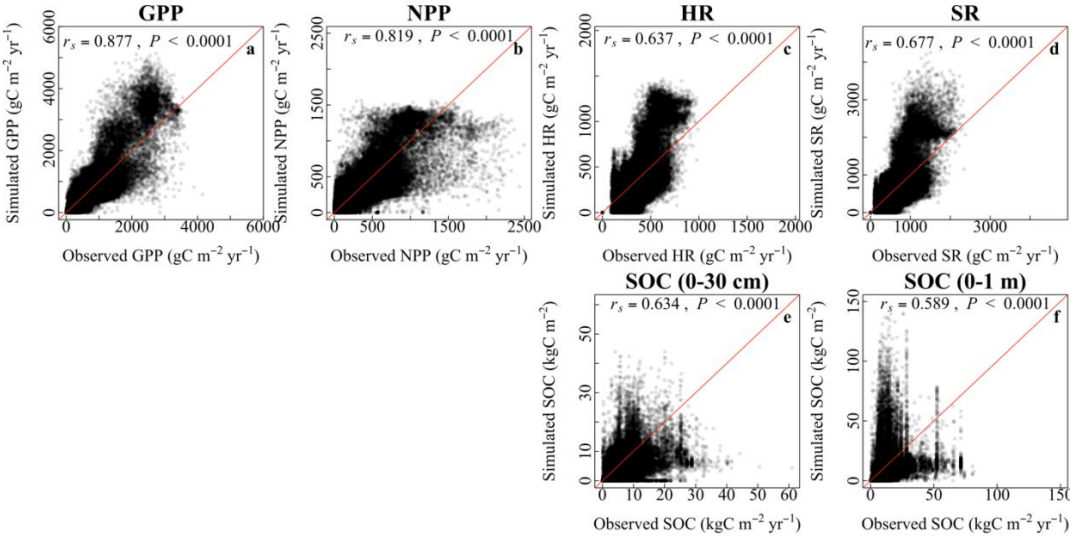

Fig. 4. Grid-by-grid comparison between observed and the CLM4.5-simulated grid cells of (a) GPP, (b) NPP, (c) HR, (d) SR, € SOC in the top 30 cm, and (f) SOC in the top 1 m. Red lines are 1:1 line. GPP: gross primary productivity; NPP: net primary productivity; HR: heterotrophic respiration; SR: soil respiration; SOC: soil organic carbon.

1095

https://doi.org/10.5194/bg-2023-15
Preprint. Discussion started: 1 March 2023

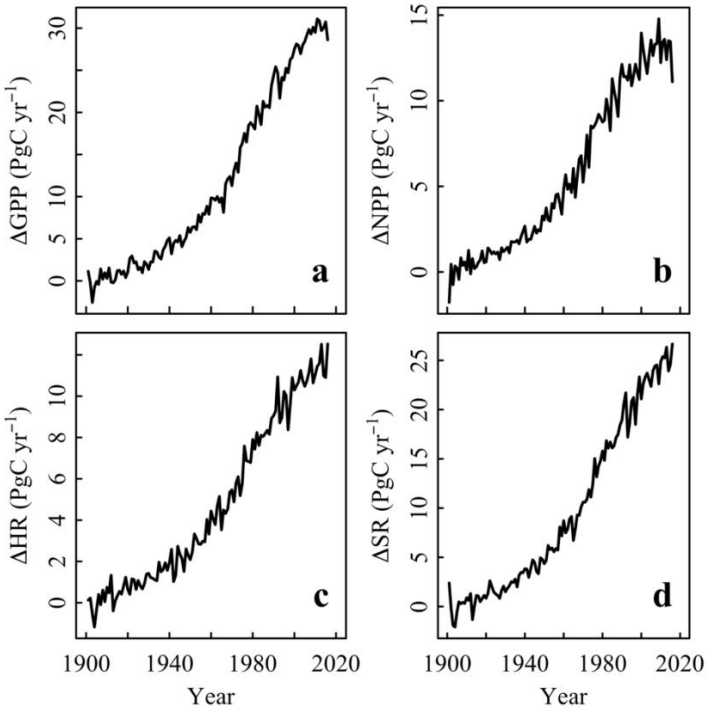

Fig. 5. Evolution of annual carbon flux of area-weighted (a) GPP, (b) NPP, (c) HR, and (d) SR simulated by the CLM-Microbe model since 1901. The baseline was the ten-year average of corresponding variables during 1901-1910. GPP: gross primary productivity; NPP: net primary productivity; HR: heterotrophic respiration; SR: soil respiration.

1100

https://doi.org/10.5194/bg-2023-15
Preprint. Discussion started: 1 March 2023

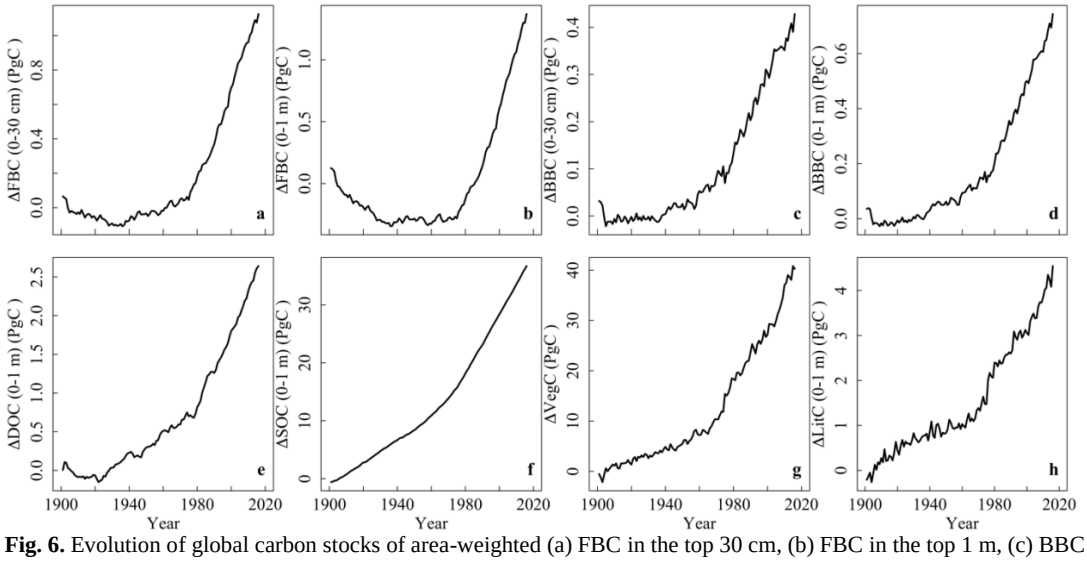

Fig. 6. Evolution of global carbon stocks of area-weighted (a) FBC in the top 30 cm, (b) FBC in the top 1 m, (c) BBC in the top 30 cm, (d) BBC in the top 1 m, (e) DOC in the top 1 m, (f) SOC in the top 1 m, and (g) VegC, and (h) LitC in the top 1 m simulated by the CLM-Microbe model since 1901. The baseline was the ten-year average of corresponding variables during 1901-1910. DOC: dissolved organic carbon; SOC: soil organic carbon; FBC: fungal biomass carbon; BBC: bacterial biomass carbon; MBC: microbial biomass carbon; VegC: vegetation carbon; LitC: litter carbon.

https://doi.org/10.5194/bg-2023-15
Preprint. Discussion started: 1 March 2023

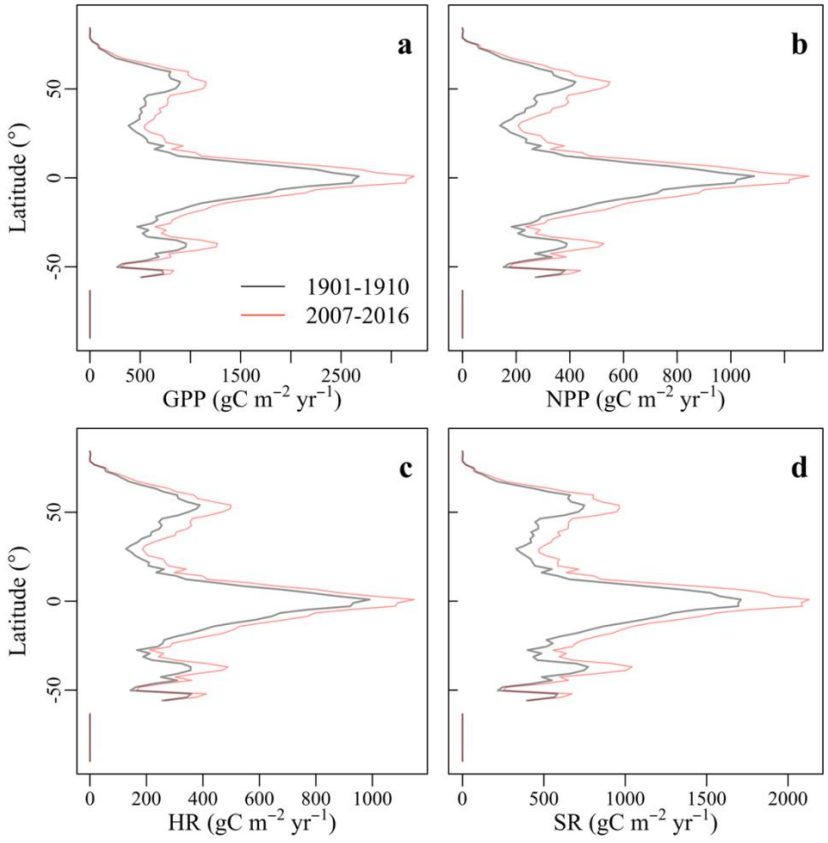

Fig. 7. Latitudinal gradients of the CLM-Microbe model simulated ten-year averages of (a) GPP, (b) NPP, (c) HR, and (d) SR during 1901-1910 and 2007-2016. GPP: gross primary productivity; NPP: net primary productivity; HR: heterotrophic respiration; SR: soil respiration.

https://doi.org/10.5194/bg-2023-15
Preprint. Discussion started: 1 March 2023

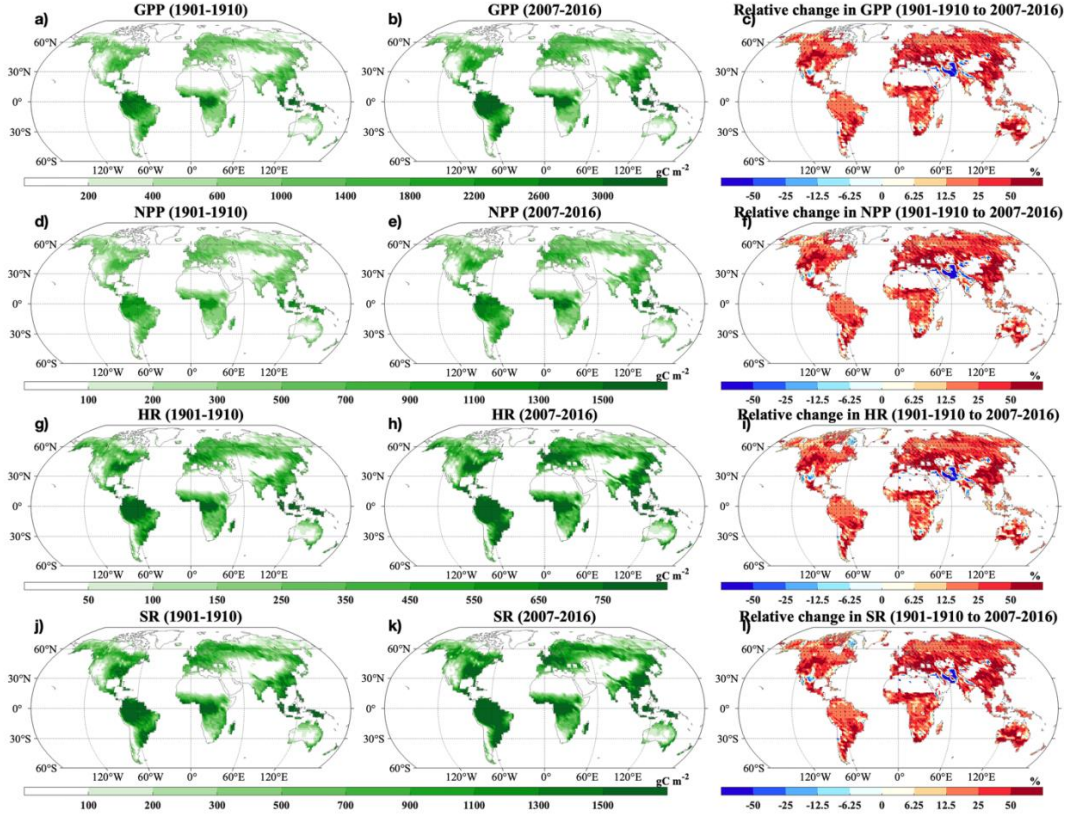

Fig. 8. Spatial distributions of decadal averages of (a-b) GPP, (d-e) NPP, (g-h) HR, and (j-k) SR during (a, d, g, and j) 1901-1910 and (b, e, h, and k) 2007-2016 and relative changes in (c) GPP, (f) NPP, (i) HR, and (l) SR by 2007-2016 relative to 1901-1910.

1115 GPP: gross primary productivity; NPP: net primary productivity; HR: heterotrophic respiration; SR: soil respiration.

https://doi.org/10.5194/bg-2023-15
Preprint. Discussion started: 1 March 2023

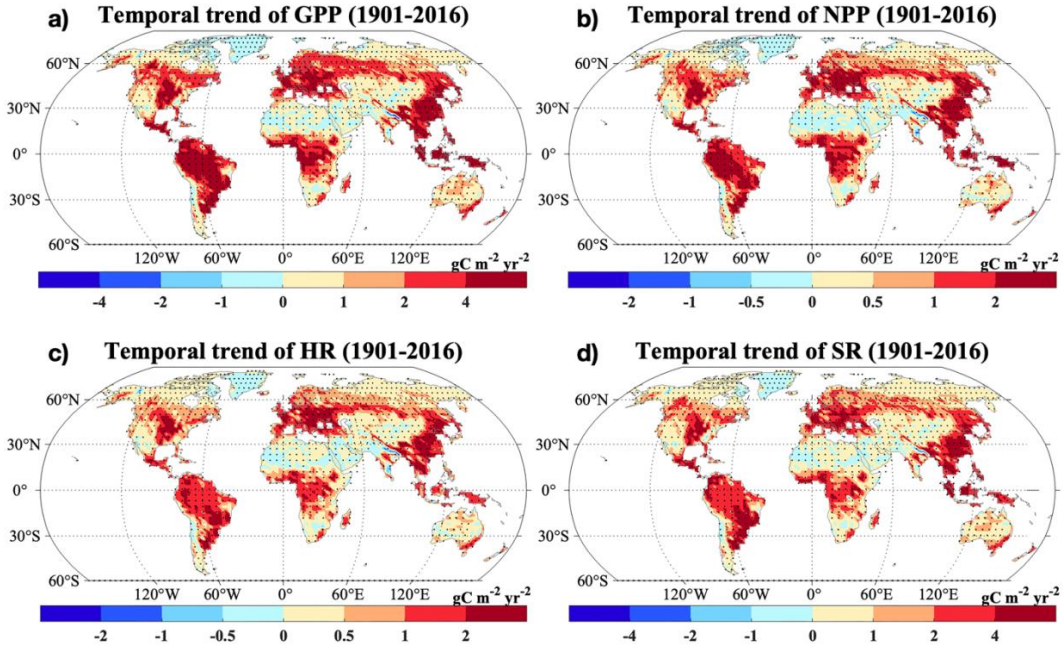

Fig. 9. Changing rates of the CLM-Microbe model simulated (a) GPP, (b) NPP, (c) HR, and (d) SR from 1901 to 2016. GPP: gross primary productivity; NPP: net primary productivity; HR: heterotrophic respiration; SR: soil respiration. Black dot in each grid indicates significant regression (P<0.05).

https://doi.org/10.5194/bg-2023-15
Preprint. Discussion started: 1 March 2023

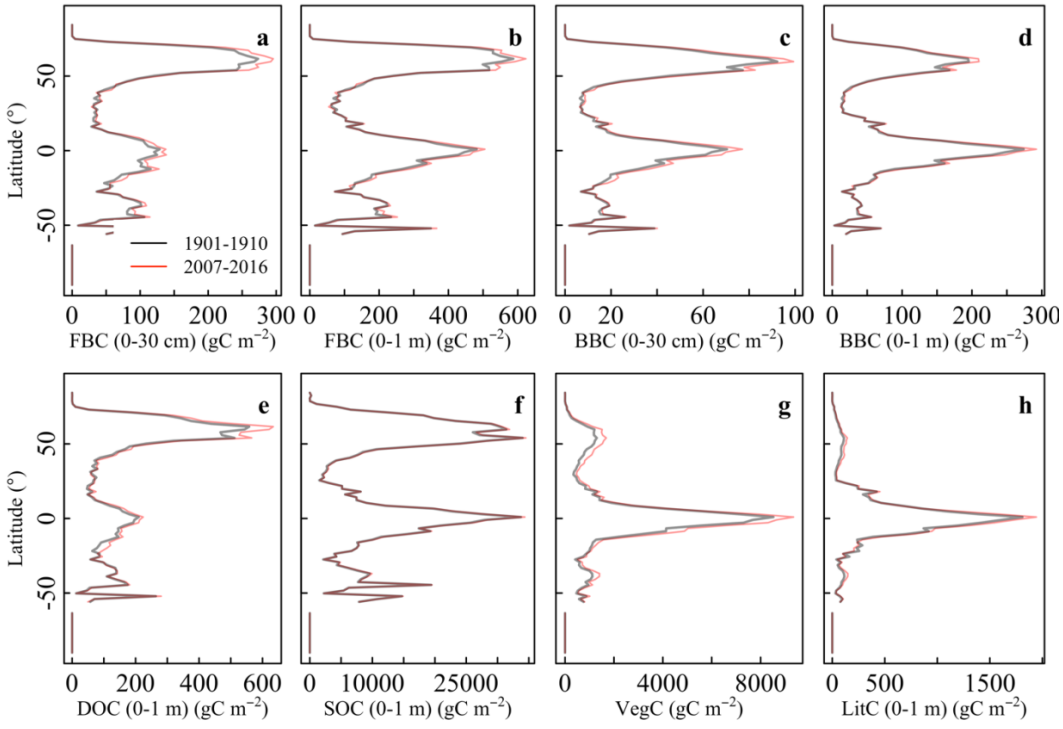

Fig. 10. Latitudinal gradients of the CLM-Microbe model simulated ten-year averages (a) FBC in the top 30 cm, (b) FBC in the top 1 m, (c) BBC in the top 30 cm, (d) BBC in the top 1 m, (e) DOC in the top 1 m, (f) SOC in the top 1 m, and (g) VegC, and (h) LitC in the top 1 m during 1901-1910 and 2007-2016. FBC: fungal biomass carbon; BBC: bacterial biomass carbon; DOC: dissolved organic carbon; SOC: soil organic carbon; VegC: vegetation carbon; LitC: litter carbon.

https://doi.org/10.5194/bg-2023-15
Preprint. Discussion started: 1 March 2023

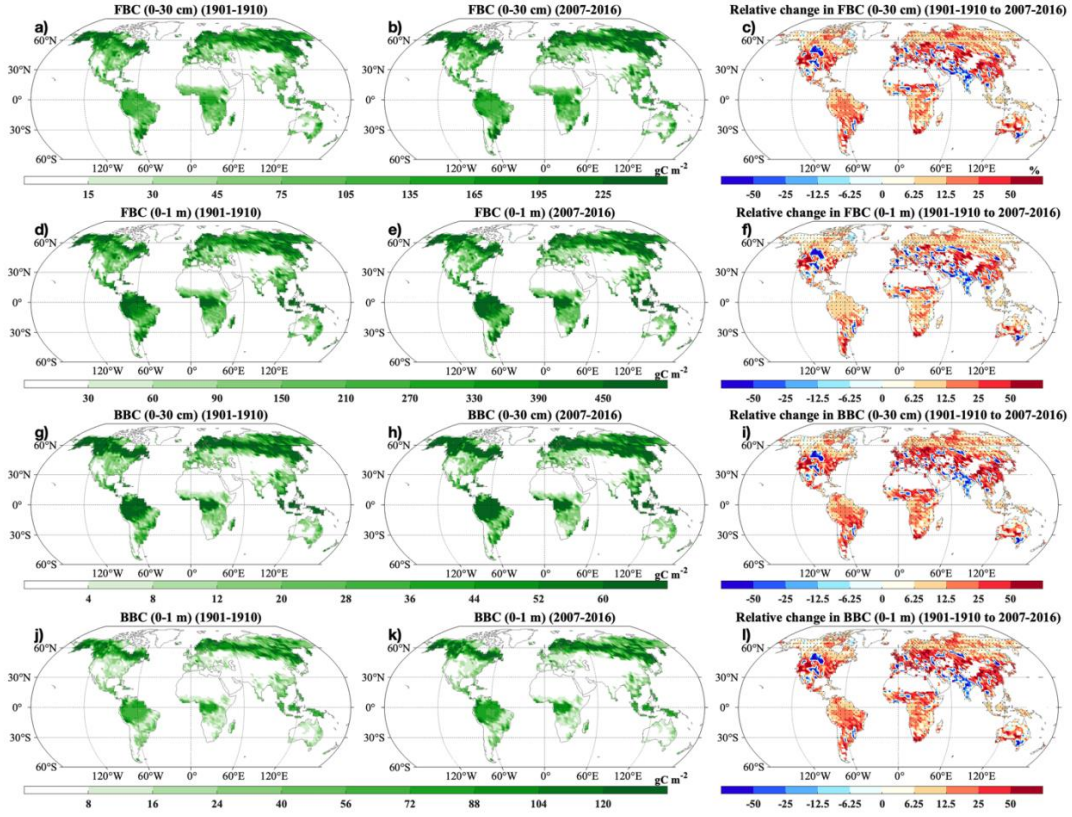

Fig. 11. Spatial distributions of decadal averages of (a-b) FBC in the top 30 cm, (d-e) FBC in the top 1 m, (g-h) BBC in the top 30 cm, and (j-k) BBC in the top 1 m during (a, d, g, and j) 1901-1910 and (b, e, h, and k) 2007-2016 and relative changes in (c) GPP, (f) NPP, (i) HR, and (l) SR by 2007-2016 relative to 1901-1910. FBC: fungal biomass carbon; BBC: bacterial biomass carbon.

https://doi.org/10.5194/bg-2023-15
Preprint. Discussion started: 1 March 2023

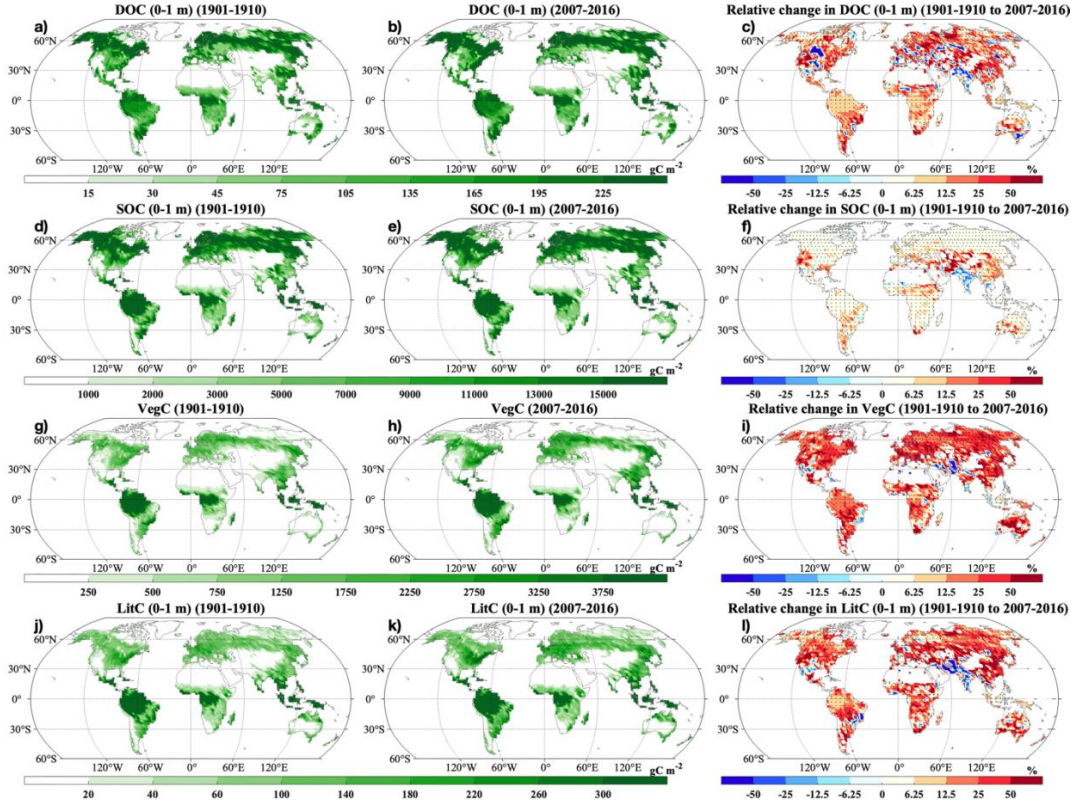

Fig. 12. Spatial distributions of decadal averages of (a-b) DOC in the top 1 m, (d-e) SOC in the top 1 m, (g-h) VegC, and (j-k) LitC in the top 1 m during (a, d, g, and j) 1901-1910 and (b, e, h, and k) 2007-2016 and relative changes in (c) DOC in the top 1 m, (f) SOC in the top 1 m, (i) VegC, and (l) LitC in the top 1 m by 2007-2016 relative to 1901-1910. DOC: dissolved organic carbon; SOC: soil organic carbon; VegC: vegetation carbon; LitC: litter carbon.

https://doi.org/10.5194/bg-2023-15
Preprint. Discussion started: 1 March 2023

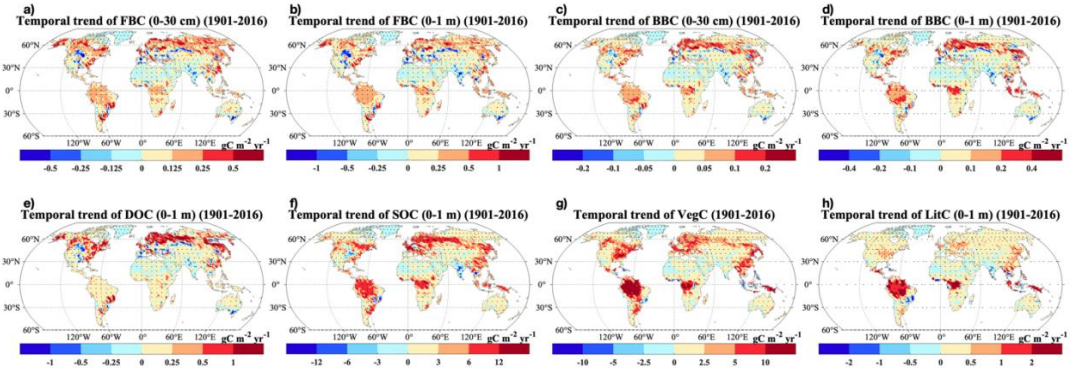

Fig. 13. Changing rates of the CLM-Microbe model simulated (a) FBC in the top 30 cm, (b) FBC in the top 1 m, (c) BBC in the top 30 cm, (d) BBC in the top 1 m, (e) DOC in the top 1 m, (f) SOC in the top 1 m, and (g) VegC, and (h) LitC in the top 1 m from 1901 to 2016. FBC: fungal biomass carbon; BBC: bacterial biomass carbon; DOC: dissolved organic carbon; SOC: soil organic carbon; VegC: vegetation carbon; LitC: litter carbon. Black dot in each grid indicates significant regression (P<0.05).

https://doi.org/10.5194/bg-2023-15
Preprint. Discussion started: 1 March 2023

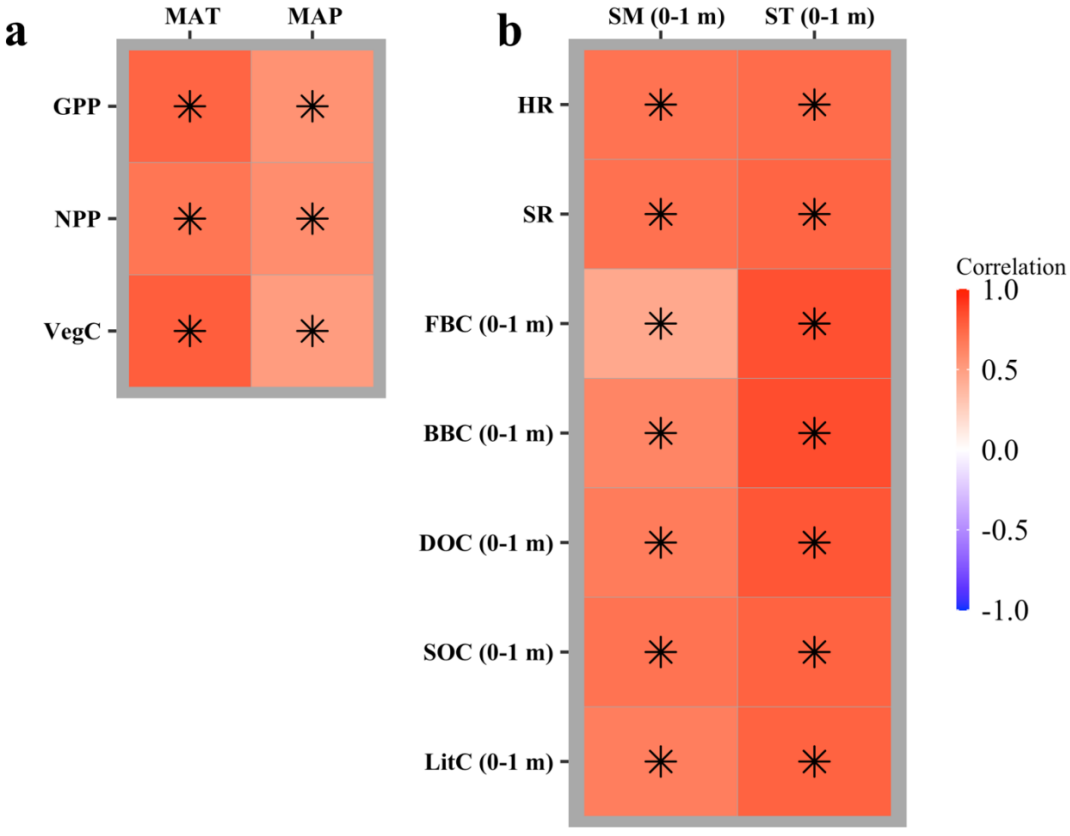

Fig. 14. Heatmap showing Pearson's correlation between the CLM-Microbe model simulated (a) GPP, NPP, and VegC and MAT and MAP and (b) HR, SR, FBC in the top 1 m, BBC in the top 1 1 m, DOC in the top 1 m, SOC in the top 1 m, and LitC in the top 1 m and SM and ST in the top 1 m from 1901 to 2016. GPP: gross primary productivity; NPP: net primary productivity; HR: heterotrophic respiration; SR: soil respiration; DOC: dissolved organic carbon; SOC: soil organic carbon; FBC: fungal biomass carbon; BBC: bacterial biomass carbon; VegC: vegetation carbon; LitC: litter carbon; MAT: mean annual temperature; MAP: mean annual precipitation; ST: soil temperature; SM: soil moisture. Black asterisks indicate significant correlations (P<0.05).

https://doi.org/10.5194/bg-2023-15
Preprint. Discussion started: 1 March 2023

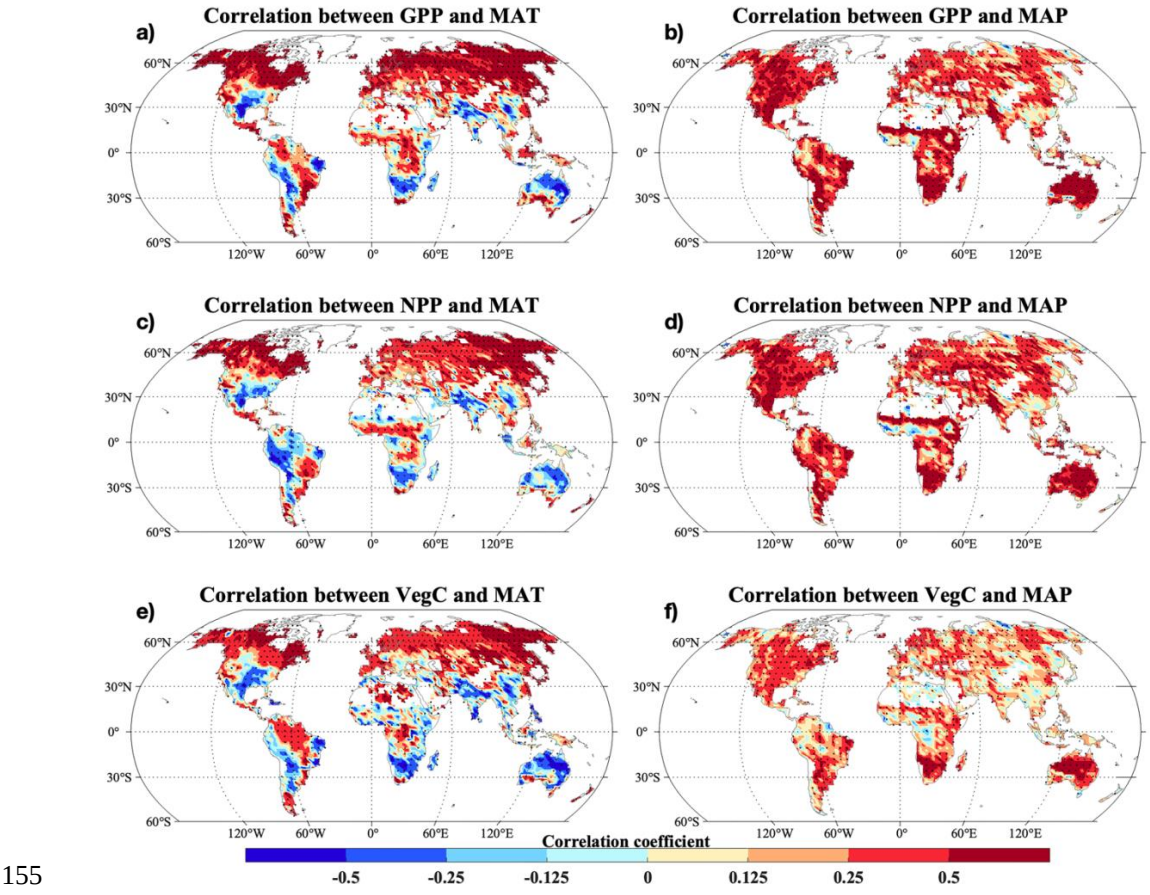

Fig. 15. Pearson's correlation between the CLM-Microbe model simulated (a-b) GPP, (c-d) NPP, and (e-f) VegC and (a, c, and e) MAT and (b, d, and f) MAP from 1901 to 2016. GPP: gross primary productivity; NPP: net primary productivity; VegC: vegetation carbon; MAT: mean annual temperature; MAP: mean annual precipitation. Black dot in each grid indicates significant correlation (P<0.05).

https://doi.org/10.5194/bg-2023-15
Preprint. Discussion started: 1 March 2023

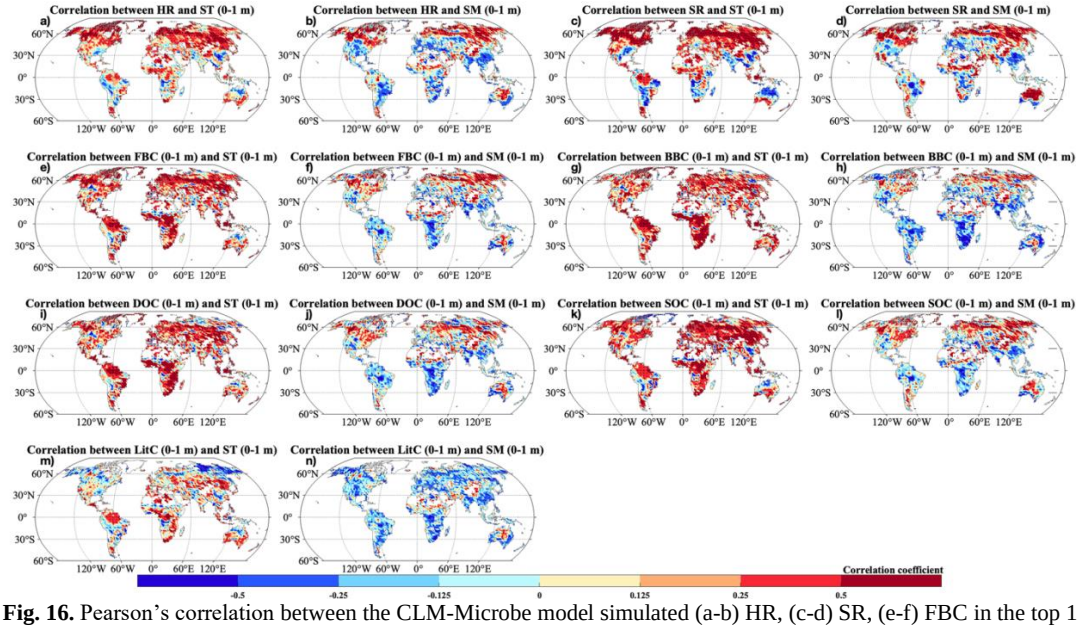

Fig. 16. Pearson's correlation between the CLM-Microbe model simulated (a-b) HR, (c-d) SR, (e-f) FBC in the top 1 m, (g-h) BBC in the top 1 m, (i-j) DOC in the top 1 m, (k-l) SOC in the top 1 m, and (m-n) LitC and (a, c, e, g, i, k, and m) ST and (b, d, f, h, j, l, and n) SM in the top 1 m from 1901 to 2016. HR: heterotrophic respiration; SR: soil respiration; FBC: fungal biomass carbon; BBC: bacterial biomass carbon; DOC: dissolved organic carbon; SOC: soil organic carbon; LitC: litter carbon; ST: soil temperature; SM: soil moisture. Black dot in each grid indicates significant correlation (P<0.05)